



REPORT

Norwegian GeoTest Sites (NGTS)

HALDEN RESEARCH SITE - SITE
CHARACTERISATION AND ENGINEERING
PROPERTIES OF HALDEN SILT

DOC.NO. 20160154-05-R

REV.NO. 0 / 2019-10-02

Neither the confidentiality nor the integrity of this document can be guaranteed following electronic transmission. The addressee should consider this risk and take full responsibility for use of this document.

This document shall not be used in parts, or for other purposes than the document was prepared for. The document shall not be copied, in parts or in whole, or be given to a third party without the owner's consent. No changes to the document shall be made without consent from NGTS.

Ved elektronisk overføring kan ikke konfidensialiteten eller autentisiteten av dette dokumentet garanteres. Adressaten bør vurdere denne risikoen og ta fullt ansvar for bruk av dette dokumentet.

Dokumentet skal ikke benyttes i utdrag eller til andre formål enn det dokumentet omhandler. Dokumentet må ikke reproduseres eller leveres til tredjemand uten eiers samtykke. Dokumentet må ikke endres uten samtykke fra NGTS.

Project

Project title: Norwegian GeoTest Sites (NGTS)
Document title: Halden research site - Site characterisation and engineering properties of Halden silt
Document no.: 20160154-05-R
Date: 2019-10-02
Revision no. /rev. date: 0

Client

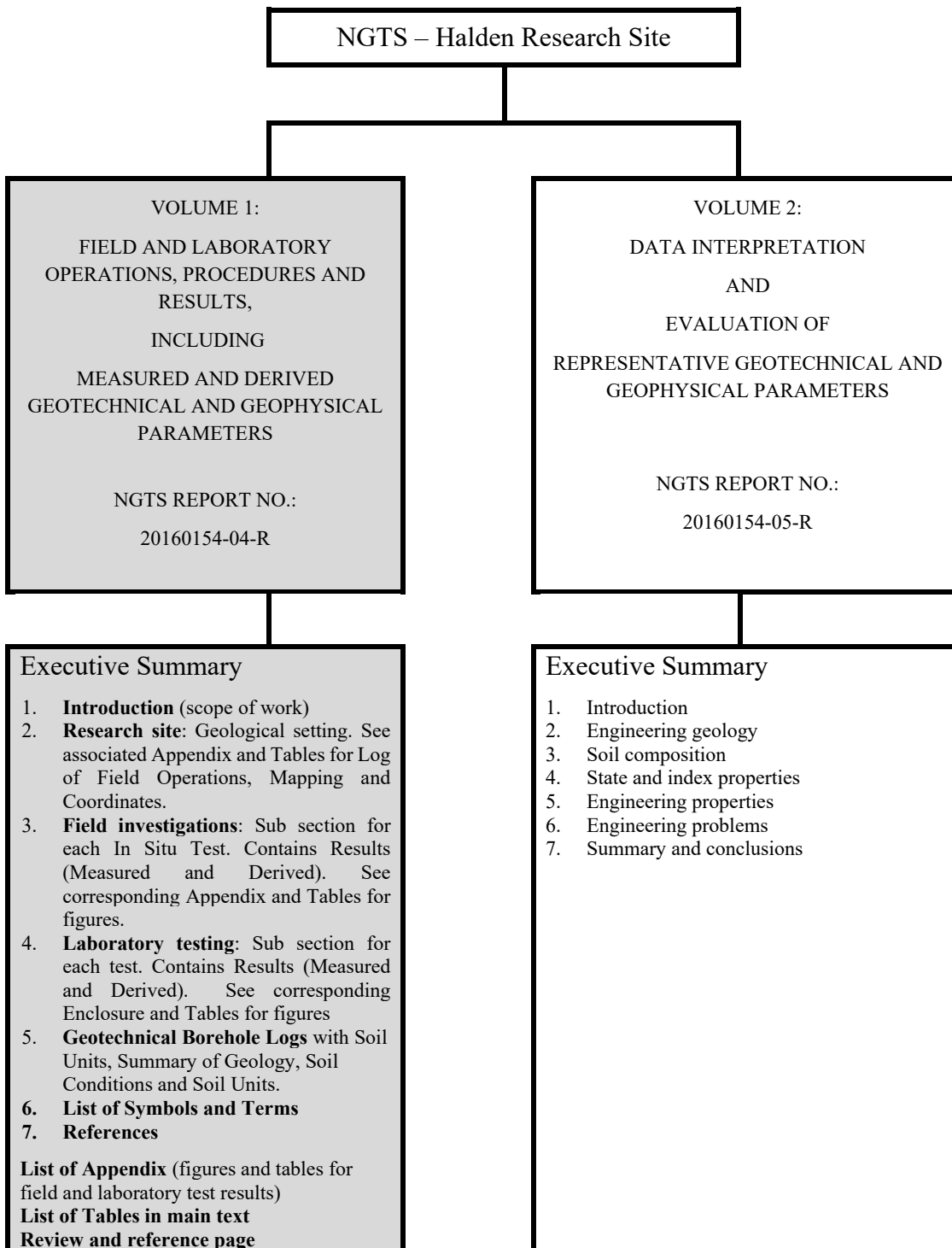
Client: Research Council of Norway (RCN)
Client contact person: Herman Fabrot
Contract reference: RCN project number 245650

for NGTS

Project manager: Jean-Sebastien L'Heureux
Prepared by: Øyvind Blaker
Reviewed by: Priscilla Paniagua

Summary

Halden silt site is property of Halden municipality and it is known locally as Rødsparken. As part of the fully characterization of Halden silt site during NGTS project, two main reports are prepared: 1) a factual report (20160154-04-R) and 2) an interpretation report (20160154-05-R) (see figure in the next page). The present report (20160154-05-R) presents an interpretation of all laboratory and in situ testing carried out for the NGTS project between May 2015 and May 2018.



White background means current report.

Contents

1	Introduction	6
2	Regional setting and methods	6
3	Engineering geology	9
3.1	Deglaciation history and depositional environment	9
3.2	Source of material	10
3.3	Stress history	11
3.4	Stratigraphy	13
4	Soil composition	18
4.1	Grain size distribution	18
4.2	Grain shape and mineralogy	19
4.3	Carbon content	19
4.4	Salinity	21
4.5	Soil fabric	22
5	State and index properties	23
5.1	Water content and Atterberg limits	23
5.2	Total unit weight and void ratio	24
5.3	Unit weight of solid particles	24
6	Engineering properties	25
6.1	In situ testing measurements	25
6.2	Overconsolidation ratio, OCR	31
6.3	Coefficient of earth pressure at rest, K_0	32
6.4	Small strain shear modulus	33
6.5	Constrained modulus	34
6.6	Coefficients of consolidation	36
6.7	Hydraulic conductivity	37
6.8	In situ undrained shear strength—field vane testing	38
6.9	In situ undrained shear strength—pressuremeter testing	39
6.10	In situ undrained shear strength—flat dilatometer testing	40
6.11	In situ strength—cone penetration testing	40
6.12	Undrained strength from laboratory testing	41
6.13	Remolded undrained shear strength and sensitivity	42
6.14	Effective stress strength parameters	45
6.15	Sample quality	46
7	Engineering problems	48
7.1	Soil sampling	48
7.2	Stress history	49
7.3	Partial drainage	50
7.4	Case history: Remmen wastewater treatment facility	51
8	Summary and conclusions	55
	References	57

Review and reference page

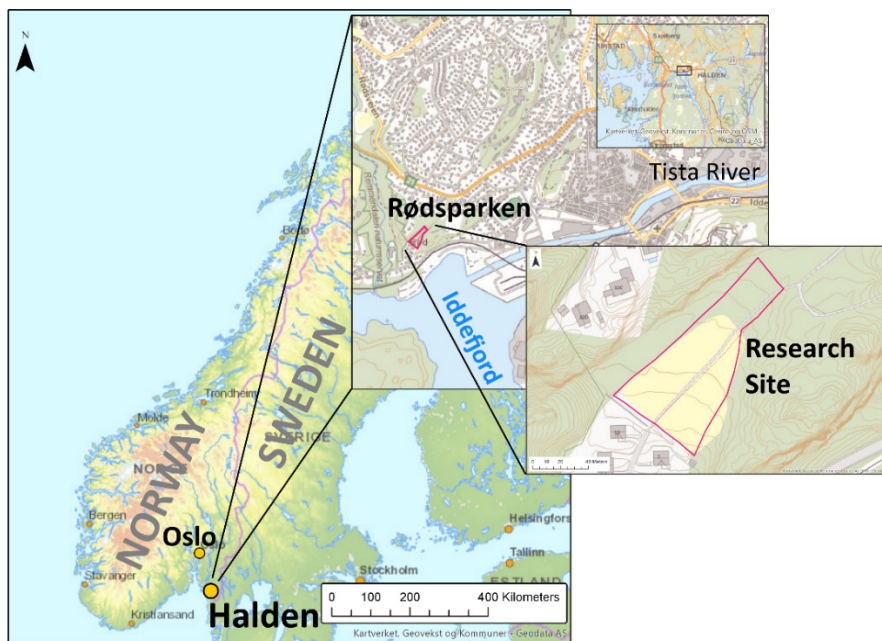
1 Introduction

Permanent geotechnical test sites provide valuable references for industry, public authorities, research organizations and academia. Some established and historic geotechnical test sites include Onsøy [1–4], Bothkennar [5], Venice lagoon [6,7], Burswood [8], Balina [9,10], UMass Amherst [11,12], and Texas A&M [13]. This paper presents the results of an extensive study of a silt site in Halden, Norway. The soil at the site was first investigated in 2011 after a local landslide nearby, following a period with significant rainfall. It was found to consist of a homogeneous, low plasticity clayey silt over soft marine clay. Silts, similar to the deposit found in Halden, but also other intermediate soils like silty sands, silty clays etc. are frequently encountered in Norwegian infrastructure projects onshore and on the Norwegian continental shelf. There is a general perception that they represent a category of challenging soils as it is difficult to obtain samples of high quality, to evaluate sample disturbance and quality, and little guidance is available on the selection of appropriate engineering properties for practical use. A widely accepted particle size classification defines silt as particles in the range of 0.002 mm and 0.063 mm [14] and these particles are typically transported by moving currents (e.g. rivers and creeks) and settle in still water. As such, silt deposits are often found all over the world in conjunction with fjords, estuaries and lakes. Therefore, the knowledge acquired at the Halden research site is of national and international importance.

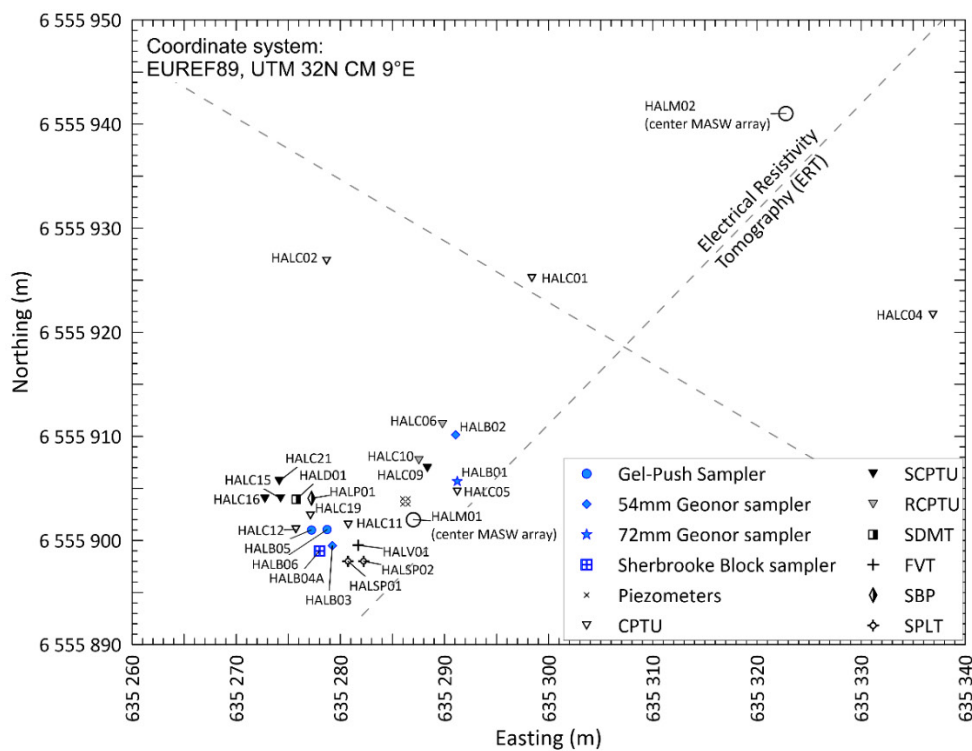
2 Regional setting and methods

Halden is located in Southeastern Norway, approximately 120 km south of Oslo, see Figure 1a. The research site is one of five National Geo Test Sites (NGTS) and located west of the city center, in what is currently a public park (Rødsparken) belonging to the Halden municipality. It covers about 6000 m² and its topography is almost flat. Elevation above mean sea level varies from +27 m to +34 m (NN2000 datum) from the southwest to northeast. Towards the north and west, the site borders a ridge which ascends to +55 m. Another ridge varying between +35 m to +44 m borders the site to the east. A residential area is found along the road Bøkerveien to the south.

The site has been characterized by combining the results of a number of geological, geophysical and geotechnical site investigation tools. A complete list of all geophysical, in situ and laboratory tests conducted at the site, with general test procedure references and key parameters are presented in Table 1. All test locations are presented on the map in Figure 1b.



(a)



(b)

Figure 1. (a) Site location, and (b) site layout. Investigated locations include resistivity and geophysical investigation tools (ERT, MASW), ground water and temperature monitoring, soil sampling using various samplers and in situ testing (CPTU, SCPT, RCPTU, SDMT, FVT, SBP and SPLT).

Table 1. Summary of geophysical, in situ and laboratory tests conducted at Halden research site, with general test procedure references and key parameters.

Test	Measured	Interpreted	Reference/Comment
Geophysical/non-intrusive			
Electrical resistivity tomography (ERT)	Resistivity	$z_{bedrock}$, soil type	
Multi-channel analysis of surface waves (MASW)	v_p, ω	V_s, G_{max}	
In situ			
Rotary pressure sounding (RPS)	F_{DT}	$z_{bedrock}$	[15]
Cone penetration test (CPTU, SCPT, RCPT)	$q_c, f_{sr}, u_2, v_{vh}, \kappa$	$\sigma'_{pr}, M, G_{max}, S_u, \phi', c_h$	[16]
Seismic flat dilatometer (SDMT)	$P_0, P_1, I_D, K_D, E_D, v_{vh}$	$S_{u,DMT}, K_0, \sigma'_{pr}, \phi'$	[17]
Self-boring pressuremeter test (SBPT)	$P_0, P_f, P_L, \varepsilon_c$	$\sigma_h, K_0, S_{u,SBP}, G_{max}$	[18]
Pore pressure	u, t	u_0	[19], Piezometers
Field vane test (FVT)	Torque	$S_u, S_{u,rem}$	[20]
Ground temperature monitoring	T, t		Thermistor string
Hydraulic fracture test (HFT)	$\Delta V, P, t$		[21]
Screw plate load test (SPLT)	δ, q_{ult}		
Sampling			
Geonor (ϕ 72 mm) fixed piston			[22]
Geonor (ϕ 54 mm) fixed piston (composite)			[22]
Sherbrooke block (ϕ 250 mm)			[22,23]
Mini-block (ϕ 150 mm)			[24]
Gel-Push (ϕ 72 mm)			[25,26]
Laboratory			
Water content	w	$\gamma_t (\rho_t)$	[27]
Unit weight (density)	$\gamma_d, \gamma_t (\rho_d, \rho_t)$		[28]
Unit weight of solid particles	$\gamma_s (\rho_s)$		[29]
Atterberg limits	$w_L (LL), w_p (PL)$	$I_p (PI), I_L (LI)$	[30]
Grain size distribution		% sand, silt, clay	[31,32]
Fall cone test	Penetration	$S_u, S_{u,rem}$	[33]
Carbon content	% TC, TOC		NGU in-house
Salinity	κ	gNaCl	[34]
X-ray diffraction (XRD)		% minerals	NGU in-house
X-ray inspection (XRI)			NGU in-house
Scanning Electron Microscopy (SEM)			
Multi sensor core logging (MSCL)	ρ_t, MS	n	NGU in-house
Split core imaging			NGU in-house

Test	Measured	Interpreted	Reference/Comment
<i>Incremental loading oedometer (IL)</i>	$t, \sigma'_v, \varepsilon$	$\sigma'_{pr}, c_G, c_v, c_{\alpha}, k_v$	[35]
<i>Constant rate of strain oedometer (CRS)</i>	$t, \sigma'_v, \varepsilon$	$\sigma'_{pr}, c_G, c_v, k_v$	[36,37]
<i>Hydraulic conductivity</i>	k_h, k_v	r_k	[36,38]
<i>Electrical resistivity</i>	<i>Resistivity</i>	κ	[39]
<i>Triaxial test: CAUC, CAUE, CK₀UC, CADC</i>	ε, q, p, u	$c', \phi, s_{uG}, s_{uE}, E$	[40,41]
<i>Direct simple shear (DSS)</i>	τ_{hr}, σ'_v	s_{uD}, G	[42,43]
<i>Bender element test (BE)</i>	V_{vh}	G_{max}	[44]

3 Engineering geology

3.1 Deglaciation history and depositional environment

Deglaciation of Southeastern Norway started at c. 16–15,000 years ago. It was interrupted at around 12,000 and 11,300 years ago by colder periods that led to re-advance of glaciers and formation of frontal moraines in the region (e.g. the “Ra” moraine). As the ice melted the land was subjected to intense isostatic uplift and relative fall of sea-level. The highest post-glacial sea level in the region (marine limit) is about 190 m above the present sea level and was formed 10,700 years ago [45]. The early Holocene period was characterized by rapid sedimentation of marine clays and silts at the site as a consequence of the rapid fall in sea-level. This was followed by more placid deposition in an estuarine/distal deltaic environment associated with the prograding Tista River delta. The shoreline reconstruction curves from the region, proposed by Klemsdal [46], show that the site most likely emerged from the marine environment c. 5,000 years ago (Figure 2). Two radiocarbon (¹⁴C) datings of marine shell fragments are available from the research site (Table 2); one from the clay at about 16.3 m depth (elevation about 12 m.a.s.l), and a second from the clayey, silt at 6.4 m depth (22 m.a.s.l). The results indicate 11,820 ± 25 years before present (BP) and 6,455 ± 25 years BP, respectively. This corresponds well with earlier carbon dating results from the area [47] and the deglaciation history. The average rate of sedimentation corresponds to about 1.0–1.4 mm/year.

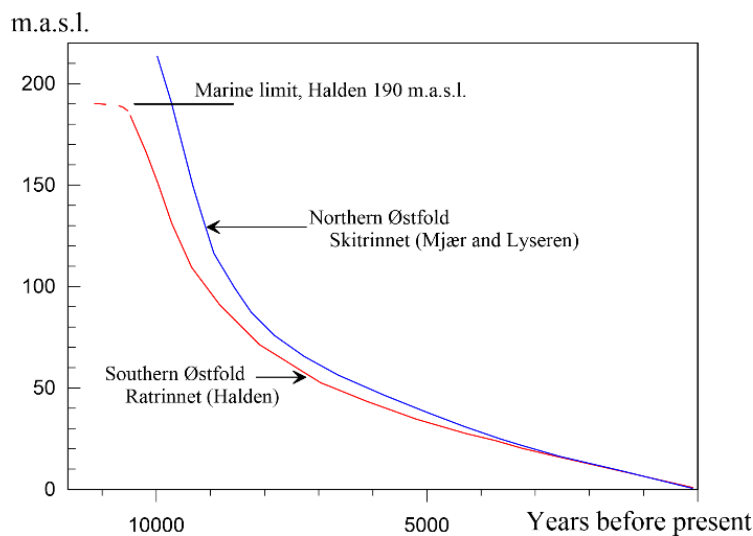


Figure 2. Shoreline reconstruction curves from Halden region (Northern and Southern Østfold), after Klemsdal [46]. The research site most likely emerged from the marine environment c. 5,000 years ago.

3.2 Source of material

Figure 3 presents the location of the research site within the regional geological setting. The Halden municipality lies within the Norwegian southeast basement area. The dominating bedrock is gneiss in the northeast and granite in the northwest and southeast [47]. Glacial striations are generally north-south and northeast-southwest and topographical characteristics such as small valleys and hills are typically oriented in that direction. The most prominent geological feature in the area is the “Ra”, an end moraine complex deposited about 11,300–10,700 years ago during the Early Younger Dryas. It traverses the region from northwest to southeast and retains the water in lakes Tvetervatn, Rokkevatnet and Korsevatnet. Earlier the moraine also retained the larger lake Femsjøen. A second zone of marginal moraine, parallel to the Ra is located south of Halden, namely the “Outer Ra”, or the Onsøy-Borge moraine. Between and outside these two features is a large veneer of clay deposits, interrupted in certain areas by silt and sand deposits, e.g. south of Halden. Areas northeast of the Ra are dominated by exposed bedrock, with clay only in local depressions. The Glomma River, Norway’s longest and largest river, runs into the Oslo fjord in the city of Fredrikstad, about 25 km northwest of the Halden research site. East of the site flows a system of lakes and rivers called “Haldenvassdraget”. This system is the second largest in Norway and runs into the Idde fjord in Halden through the Tista River (Figure 1a). During higher sea levels, the test site was likely highly influenced by both of these river systems, as Halden was inundated by the sea [48]. Thus the source of material supplied has an important contribution from the whole of southeastern Norway and has primarily been produced by glacial erosion, with secondary fluvial transport.



Figure 3. Quaternary map of the Halden area, Southeast Norway, with the research site circled in red. The colors reflect the geological processes and general properties of the deposits. Shades of blue indicate that the soils have been transported by and deposited in a marine environment. These deposits dominate the Halden area. Shades of green indicate soils that were deposited by the ice. Shades of yellow indicate fluvial deposits, and pink shows exposed bedrock. After [47].

3.3 Stress history

From the geological history of the site no known loading events have occurred. Relative to the sea level the Oslo area has been rising steadily, and soil units were deposited during a single period of submergence [49]. The depositional history hence suggests that the soil at the site is likely to be geologically normally consolidated, except perhaps for some surface weathering, desiccation and aging. Substantial erosion is unlikely to have occurred, but seasonal ground water and temperature fluctuations may cause some apparent preconsolidation. Data from one standpipe and four electrical piezometers installed at 5 m, 10 m, 15 m and 20 m depth reveal that the ground water table is located at about 2 m depth and that the in situ pore pressure, u_0 (two year average—October 2016 to October 2018), is close to hydrostatic in the silt units and sub-hydrostatic in the clay layer below (Figure 4a). Sub-hydrostatic pore pressures can occur at sites located on a hill where vertical recharge into a low permeability clay layer is less than discharge occurring away (radially) from the site in an underlying higher permeability soil unit [50]. At Halden no such permeable material has been identified below the clay. However, fractured bedrock or a thin layer of gravel could facilitate radial drainage away from the site. The piezometer logs, presented in Figure 4b, demonstrate how the

fluctuating ground water table causes peak pore pressures during winter and after the spring snow melt (February to May), and pore pressure lows at the end of the summer (August). These fluctuations cause seasonal changes in the mean effective stresses in the order of 5–10 kPa.

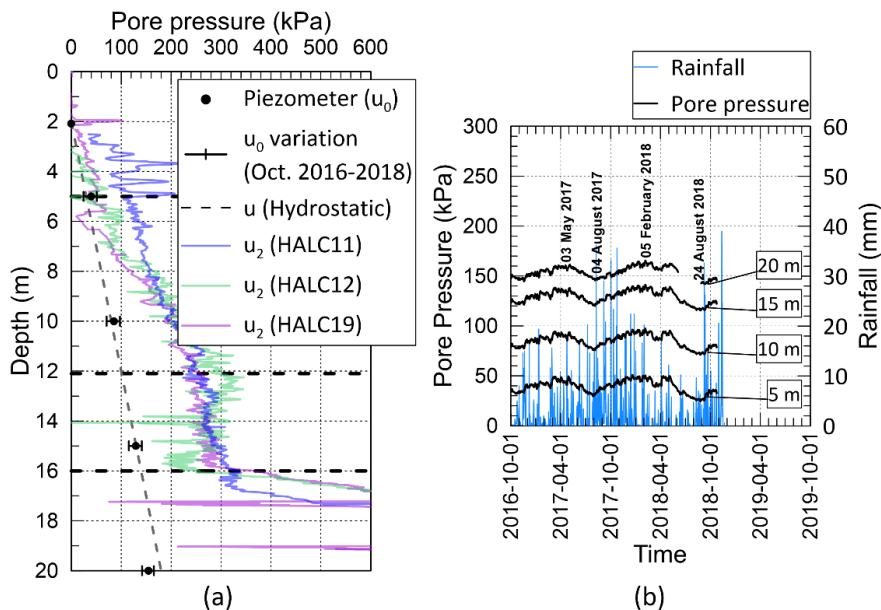


Figure 4. (a) Pore pressure from in-situ piezometers (locations HALP01-HALP04) and u_2 from CPTU (locations HALC11, HALC12 and HALC19). The dotted line indicates the theoretical hydrostatic pore pressure acting from 2 m depth. (b) In-situ pore pressure measured by four electric piezometers installed at 5 m, 10 m, 15 m and 20 m depth, and rainfall in the area, October 2016 to October 2018.

Temperature fluctuations in the order of 20° Celsius are observed in the top soil throughout the year. However, below about 6 m depth the fluctuations are negligible and the temperature is fairly constant with depth at about 8 degrees Celsius (Figure 5).

From the total unit weights (γ ; Section 5.2) and the in situ pore pressure depicted in Figure 4a the total and effective vertical stress conditions (σ_{v0} , σ'_{v0}) are derived and plotted in Figure 6. The total stress profile is approximated by using $\gamma = 19 \text{ kN/m}^3$ in Units I and II, and $\gamma = 20 \text{ kN/m}^3$ in Units III and IV. Interpretation of the apparent preconsolidation stress, or yield stress σ'_p (p'_c), from oedometer tests on silt is challenging. This is discussed in Section 6.2.

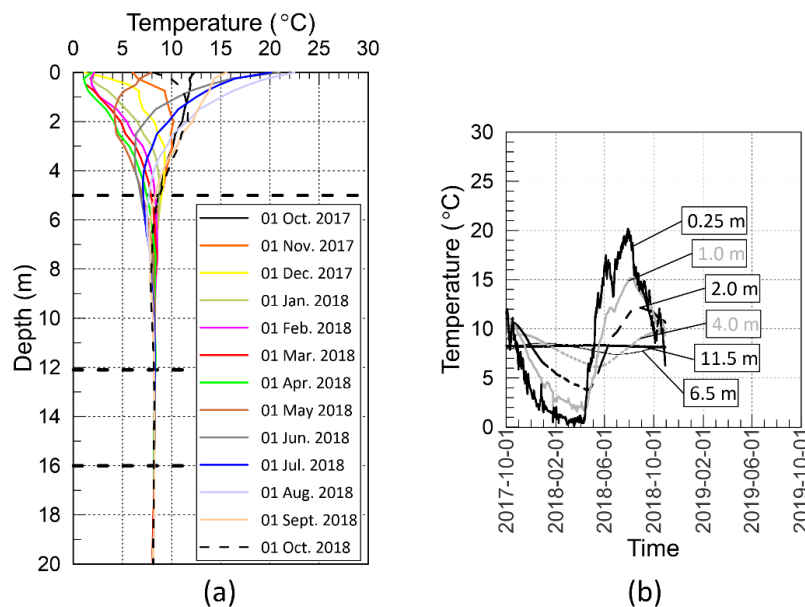


Figure 5. Thermistor string temperature log in location HALB05; (a) with depth at selected dates, and (b) with time since October 2017.

3.4 Stratigraphy

Soil layering across the site has been assessed by combining the results of a number of site investigation tools. Table 2 presents the Halden site stratigraphy, unit description with images of selected samples from the X-ray inspection (XRI) and split core imaging performed by the Geological Survey of Norway (NGU). The XRI system consists of an X-ray tube, an image intensifier and a high quality digital camera. The resulting images can be used to assess e.g. (i) soil type; (ii) soil macro fabric; (iii) the presence of inclusions such as stones, shells, sandy zones and root holes etc.; (iv) the presence of fissures, shear planes, discontinuities etc.; (v) degree of bioturbation; and (vi) indications of sample disturbance. The soil sample is placed between the X-ray tube and the image intensifier and different sections can be inspected by rotating the tube and sliding the assembled XRI configuration horizontally along the sample. Repeated runs produced three 16 bit greyscale images with 0, 45, and 90 degree axial orientation. X-ray transparency of a sediment is strongly influenced by the grain-size and the images are generally light grey for the fine-grained soils and dark grey for coarse-grained soils. The two split core images per sample were captured directly after opening using 20 ms and 40 ms exposure time.

Based on an overall interpretation of the geophysical, in situ testing and laboratory testing results the site stratigraphy is divided into four main soil units numbered Units I to IV, as depicted in Figure 7a to Figure 7g. The stratigraphy presented in the following describes the soil units as they have been identified in the southernmost part of the test site, i.e. beneath the main cluster of investigated locations shown in Figure 1b: A silty,

clayey sand constitutes the top soil and extends down to about 4.5 to 5 m depth (Unit I). It is generally loose to medium dense with some organic material (0.25%–0.5% total organic carbon). Unit I rests above a clayey silt which extend down to about 15–16 m depth. This clayey silt is separated into two soil units (Unit II and III) based on the results of in situ and index tests, but is regarded as the same material with the same geologic origin. Index and in situ tests reveal that the silt becomes sandier closer to the lowermost soil unit, Unit IV, which consists of a low to medium strength clay. This soil unit has a slightly laminated structure, with occasional shell fragments and drop stones. Depth to bedrock dips sharply from the northeast to southwest, but is typically identified at 21 m depth in the southern part of the site (see Figure 8).

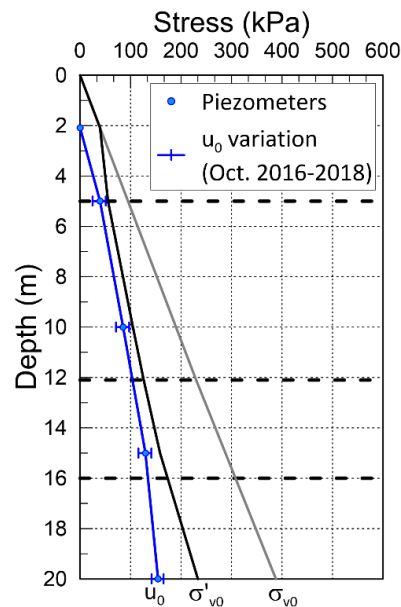
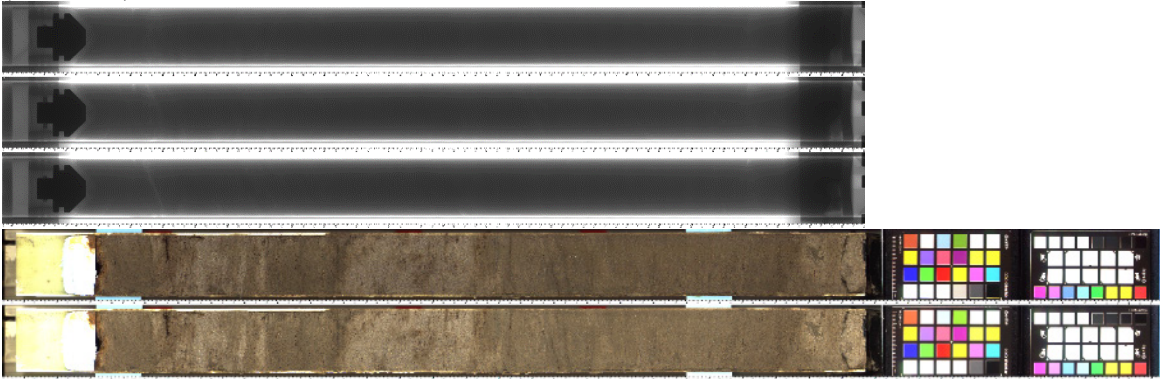
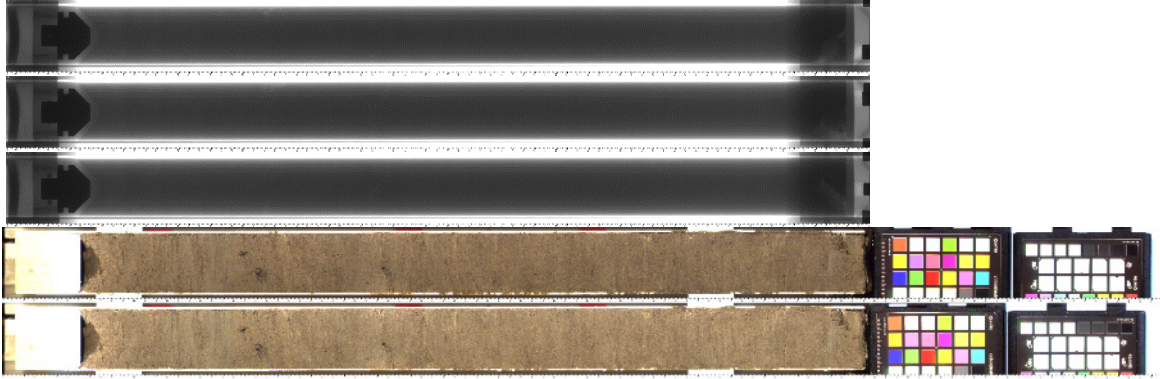
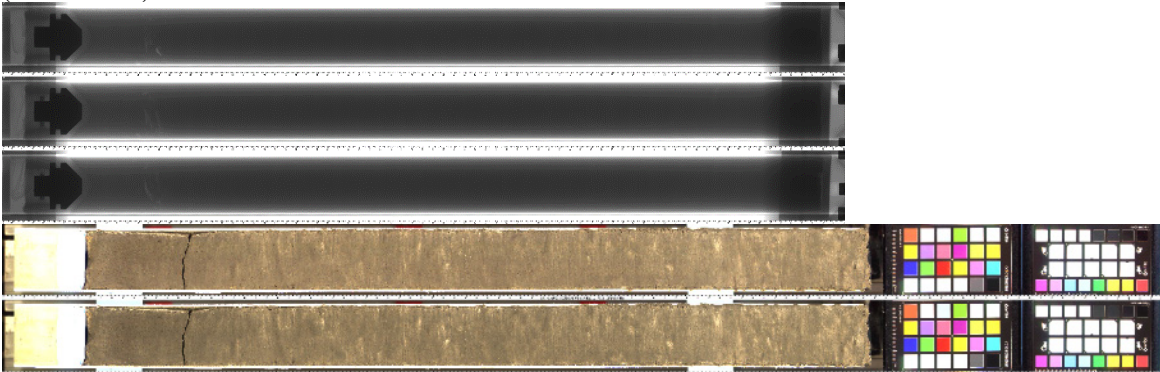
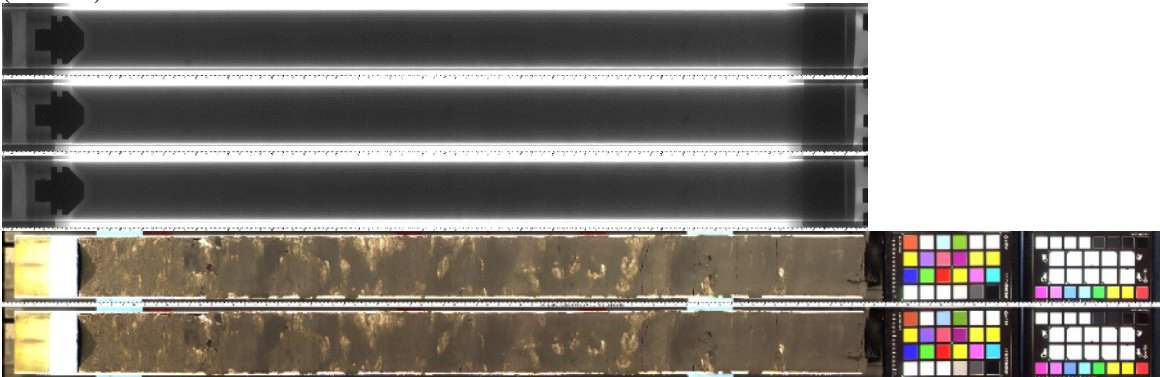


Figure 6. In-situ stress conditions (u_0 , σ_{v0} and σ'_{v0}).

Table 2. Summary of Halden stratigraphy, with X-ray images at 0°, 45° and 90° degree axial orientation, and split core images at 20 ms and 40 ms exposure time.

Depth range [m]	Soil description and imaging [-]	Comment [-]
0.0–4.5	<p data-bbox="465 376 1402 432">SAND, clayey, silty, fine, loose to medium dense, with organic material, brownish grey (Soil Unit I)</p> 	<p data-bbox="1671 448 1984 512">X-ray and split core imaging depth: 3.0–3.9 m</p>
4.5–12.1	<p data-bbox="465 871 1599 935">SILT, sandy, clayey, low to medium strength, homogeneous, mottled, occ. shell fragments, brownish grey (Soil Unit II)</p> 	<p data-bbox="1671 871 1984 1015">¹⁴C age @ 6.4m: 6,455 ± 25 years BP X-ray and split core imaging depth: 4.8–5.6 m</p>

Depth range [m]	Soil description and imaging [-]	Comment [-]
12.1–16.0	SILT, sandy, medium to high strength, homogeneous, highly bioturbated, mottled, occ. shell fragments, occ. black organic material, brownish grey (Soil Unit III) 	X-ray and split core imaging depth: 12.0–12.8 m
16.0–21.3	CLAY, silty, low to medium strength, slightly laminated, occ. shell fragments, occ. drop stones (Unit IV) 	^{14}C age @ 16.3 m: $11,820 \pm 25$ years BP X-ray and split core imaging depth: 15.6–16.4
21.3	BEDROCK	

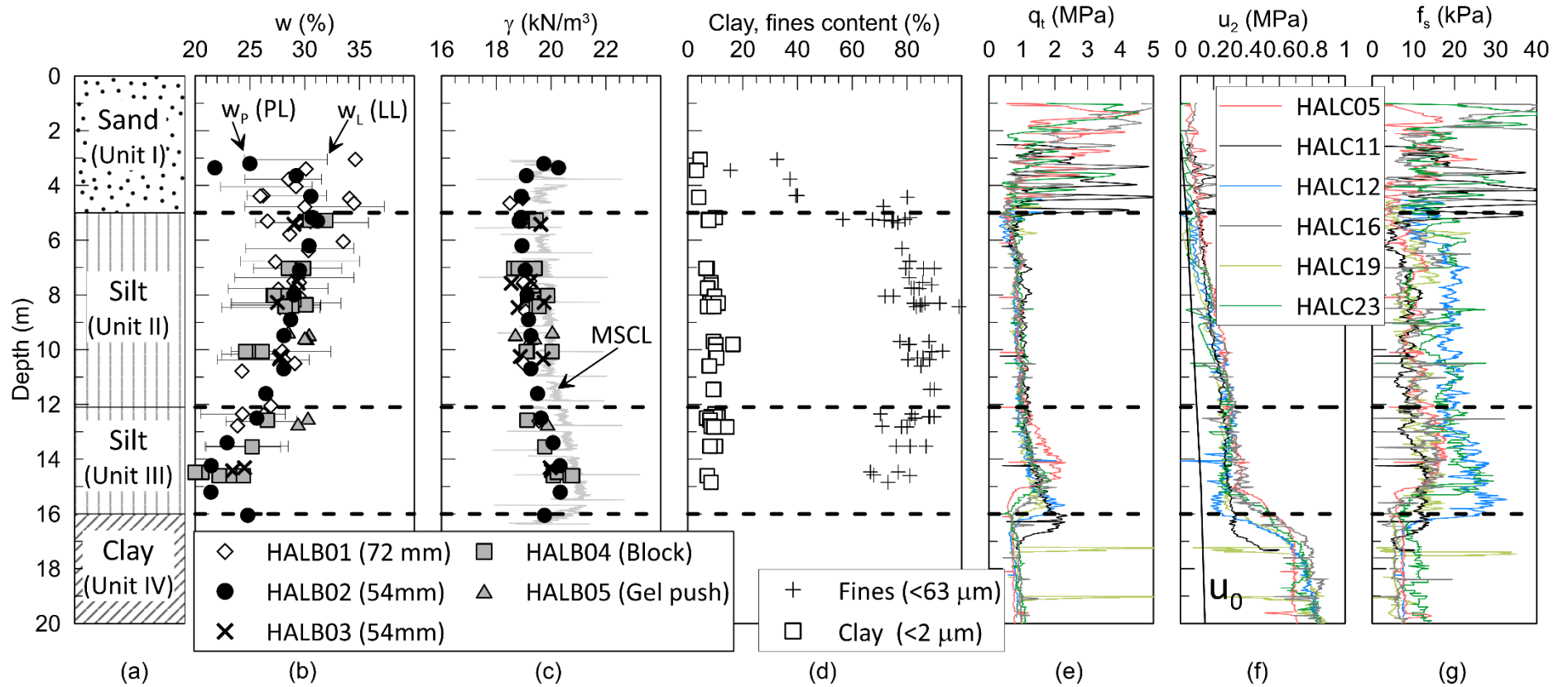


Figure 7. Classification and CPTU data; (a) Soil units, (b) natural water content and Atterberg limits, (c) total unit weight, (d) clay particle and fines content, (e) corrected cone resistance, q_v , (f) pore pressure, u_2 , and (g) sleeve friction, f_s .

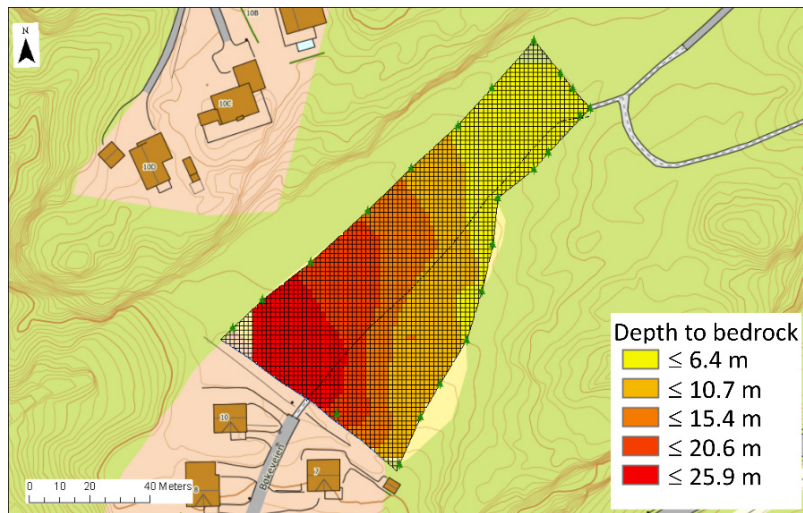


Figure 8. Approximate depth to bedrock across the research site.

4 Soil composition

4.1 Grain size distribution

Figure 9a presents two grain size distribution curves from Unit I and a typical range of grain size distributions in the silt from Units II and III. All results below 5 m depth were determined using the hydrometer method [32] or the falling drop method [31]. A summary of the clay size particle content ($d < 0.002$ mm) and fines content ($d < 0.063$ mm) with depth are presented with other classification parameters in Figure 7. The upper soil Unit I mainly consists of a silty, clayey sand. The fines content in the two silt units (Units II and III) is generally higher than 80%, slightly decreasing towards the interface with the clay in Unit IV. The clay content ($d < 0.002$ mm) is fairly constant at around 8% in Units II and III, classifying this as a clayey silt according to ISO 14688-1 [14] and the Norwegian Geotechnical Society (NGF) soil classification triangle [51] in Figure 9b. However, based on the plasticity properties of the soil (see Section 5.1) the Unified Soil Classification System (USCS) classifies these soils as silty clay with sand to lean clay with sand. No grain size data has yet been acquired in the clay layer Unit IV.

4.2 Grain shape and mineralogy

Scanning electron microscope (SEM) images in Figure 10 and Figure 11, from 6.4 m and 8.6 m depth respectively, demonstrate that the silt particles are largely angular [52]. Table 3 presents the results of three X-ray diffraction (XRD) analyses performed by the Geological Survey of Norway (NGU) on particles from Unit II and III. The results reveal very similar mineralogical content with depth. Both Units II and III contain similar amounts of quartz, plagioclase, clay minerals and mafic minerals (amphibole). These results are consistent with mineralogical analyses of the sand and silt fractions of the glacial tills examined in the region west of the Oslo fjord [53]. The clay minerals are illite and chlorite, and the presence of expanding clay minerals are low or absent.

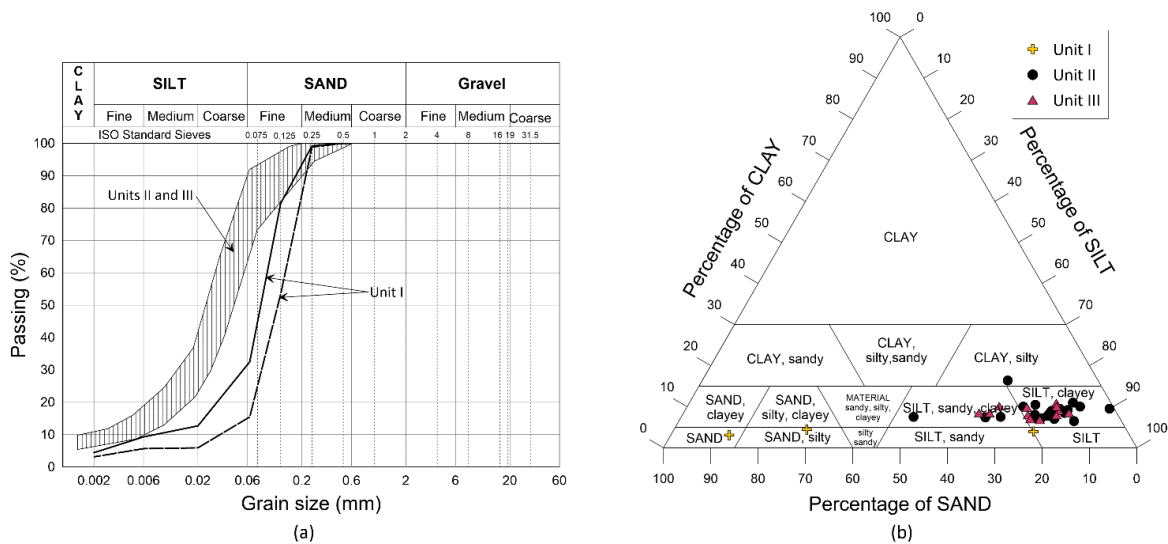


Figure 9. Classification data; (a) typical grain size distribution curves for Unit I, and Units II and III. (b) Soil classification triangle [51], which suggests 14 soil classes based on the percentage of clay, silt and sand particles.

4.3 Carbon content

Total carbon (TC) and Total Organic Carbon (TOC) were determined by dry combustion at NGUs laboratory using a LECO SC-632 analyzer with an infrared (IR) detector (Leco Corp., St. Joseph, MI). The carbon content in the silt units is generally low. Figure 12 shows that in Unit II the average TC was 0.49% with a range from 0.43%–0.54%. In Unit III the average TC is 0.24%, ranging from 0.19%–0.28%. Meanwhile the TOC in Unit II average is 0.46% while the average is lower in Unit III at a value of 0.22%.

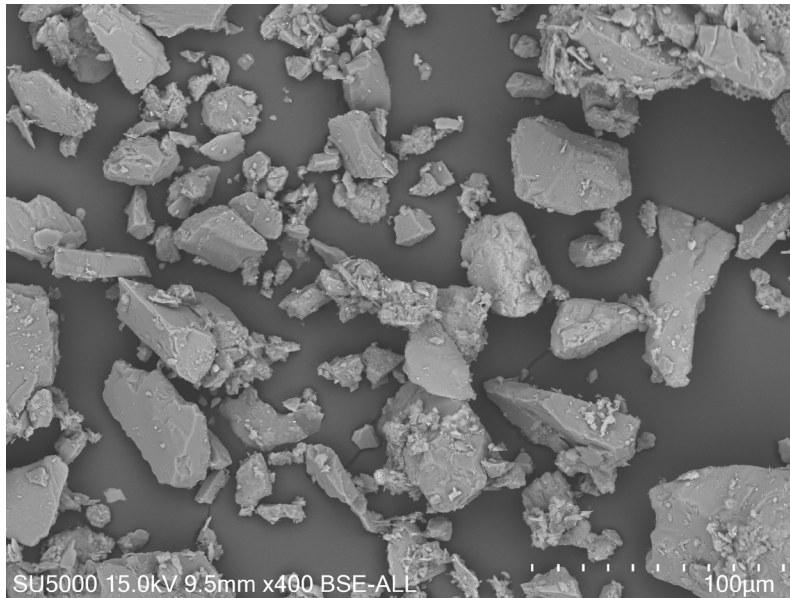


Figure 10. SEM from 6.4 m depth.

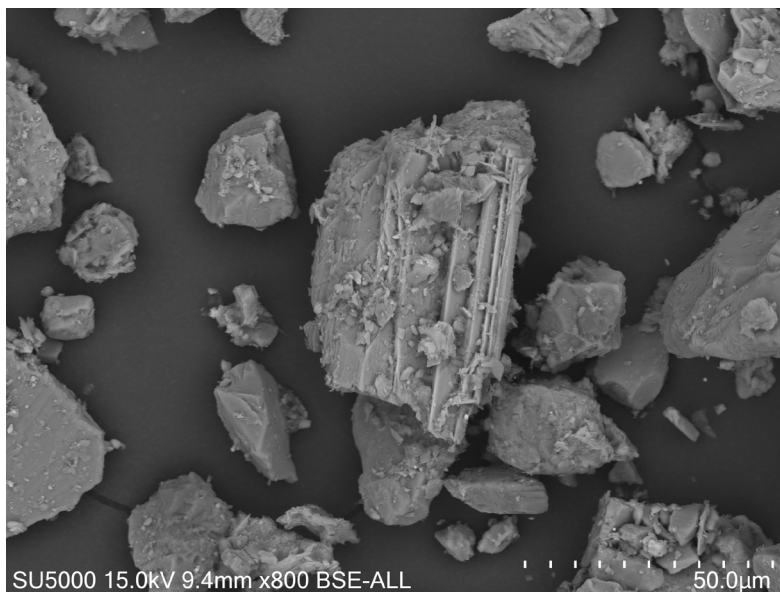


Figure 11. SEM from 8.6 m depth.

Table 3. Results of X-ray diffraction analyses on 3 specimens from Halden research site.

Unit	Depth	Quartz	Potassium Feldspar	Plagioclase	Muscovite/Illite	Chlorite	Amphibole	Pyrite
-	m	%	%	%	%	%	%	%
II	6.2	41	12	30	8	3	6	trace
II	9.5	40	13	29	8	4	6	trace
III	13.5	44	12	30	7	2	5	trace

4.4 Salinity

Nine salinity tests were performed in the laboratory by means of electrical conductivity (κ) to determine the NaCl equivalents of the pore water according to ISO 11265 [34]. Electrical resistivity tomography (ERT) profiles were conducted at the site by injecting a current into the subsurface through steel electrodes, installed 10–20 cm into the ground, and the apparent resistivity distribution along a profile or area was measured. Direct measurements of resistivity were also made during cone penetration testing at locations HALC06 and HALC10, using a resistivity add-on module with the original cone (RCPTU). The adapter consisted of an array of four ring electrodes in a Wenner configuration with equal (0.25 m) spacing between the electrodes. The RCPTU depth was corrected for the distance between the electrodes and the cone tip.

The laboratory salinity tests indicate electric conductivity (inverse of resistivity) in the range of 119 $\mu\text{S}/\text{cm}$ to 485 $\mu\text{S}/\text{cm}$, which corresponds to NaCl equivalents of 1.1 to 4.6 g NaCl/L. These results are converted to resistivity and plotted with results of measurements conducted on selected triaxial test specimens in Figure 12d. Indications from the RCPTUs at locations HALC6 and HALC10, as also presented in Figure 12d, are that the laboratory measurements are on the low side of the in situ measurements. The in situ resistivity decreases from about 300–1000 Ωm in the top soil to a fairly constant value of 100–150 Ωm in the silt. There is fair agreement between the RCPTU and ERT profiles, indicating that the in situ resistivity measurements can be considered more reliable than the laboratory measurements. The change in resistivity is linked to the reduction in salt content, and considering the fact that the soil at the site was deposited in a post glacial fjord-marine environment, leaching of the silt is likely to have occurred due to rainfall and snow melting in the Halden region. It has been suggested for Norwegian clays, that unleached marine clays have resistivities in the range of 1–10 Ωm while fully leached, potentially quick clay deposits, clayey moraine and silty sediments typically have resistivities in the range of 10–100 Ωm [54,55].

4.5 Soil fabric

Soil Units II and III are generally homogeneous, structureless to mottled, with primary bedding and laminations almost absent due to bioturbation. Such structureless soils are common in fjord-marine environments subjected to hemipelagic sedimentation and seafloor biological activity [56]. The XRI images (see Table 2) appear to confirm that that mottling is associated with internal reworking of the sediments and consequently with the partial or complete loss of any primary sedimentary bedding structures. In contrast, Unit IV shows some weak laminations and the occasional presence of drop stones (sand/gravel particles) interpreted as ice rafted debris (IRD). There is some evidence of shell fragments and iron sulphide spots, resulting from decomposition of organic matter. No evidence of cementation or fissures has been found in either of the soil units.

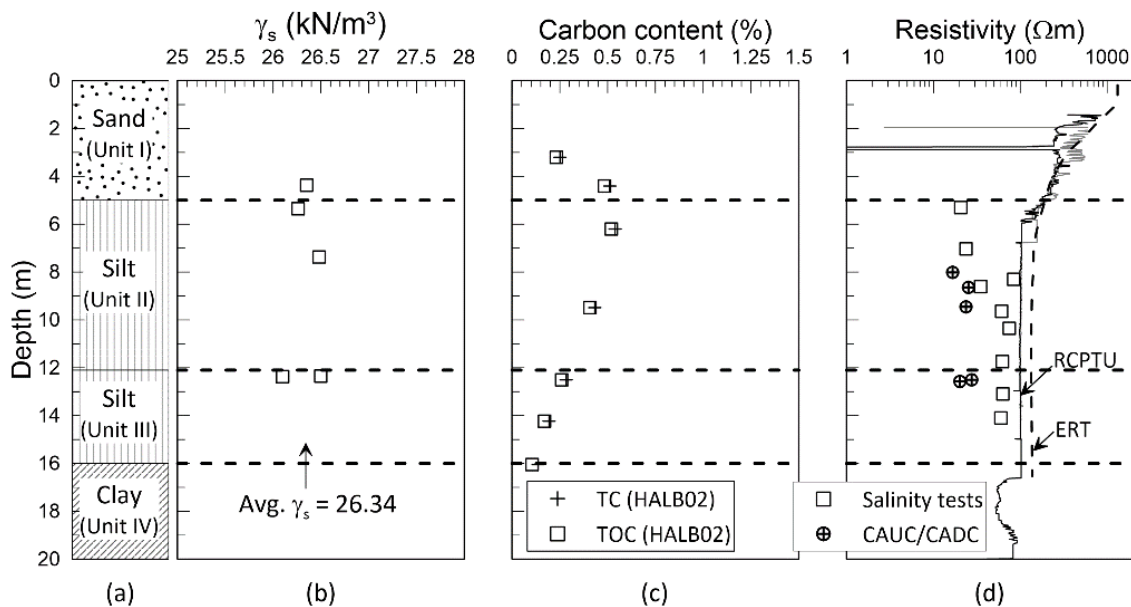


Figure 12. (a) Soil units, (b) unit weight of solid particles, (c) TC and TOC, and (d) resistivity from laboratory and field measurements.

5 State and index properties

5.1 Water content and Atterberg limits

The measured natural water contents (w) are somewhat scattered, but generally decrease with depth from about 31% at 4 m depth to about 26% at 16 m (Figure 7b). The scatter is thought to be due to different sampling techniques, and the fact that different measurements have been made over several years, i.e. certain samples may have experienced some loss of moisture during storage. Results from measurements made on the same day on samples from HALB02 all show a consistent trend decreasing with depth. While in Unit II the results generally fall between 26% and 32% the water content in Unit III decreases with depth from about 26% at 12 m depth to about 21% at 15 m. The decreasing water content with depth in Units II and III coincides with a decreasing organic content (TOC) and increasing total unit weight of the soil (See Sections 4.3 and 5.2, respectively).

The liquid limit (w_L), as measured using the fall cone, and plastic limit (w_p) were conducted in accordance with ISO 17892-12 [30]. In Unit II w_L and w_p varies between 28% and 37%, and 22% and 25%, respectively. Average plasticity index (I_p) in this soil unit is 9.3%. In Unit III w_L varies between 25% and 29%, w_p ranges from 20% to 23% and average plasticity index is 6.6%. Figure 13 shows that the results generally plot on and above the A-line in a Casagrande plasticity chart, just on the division between the inorganic low plasticity clay (CL) and inorganic silts (ML). The known differences in liquid limit, as determined by means of the fall cone and Casagrande cup for low I_p soils would likely have shifted the Halden silt data points down and left in the plasticity chart, if the Casagrande cup was used [57]. As such, a data point from the fall cone that plots on or just above the A-line could shift to below the A-line if the liquid limit was measured using a Casagrande cup.

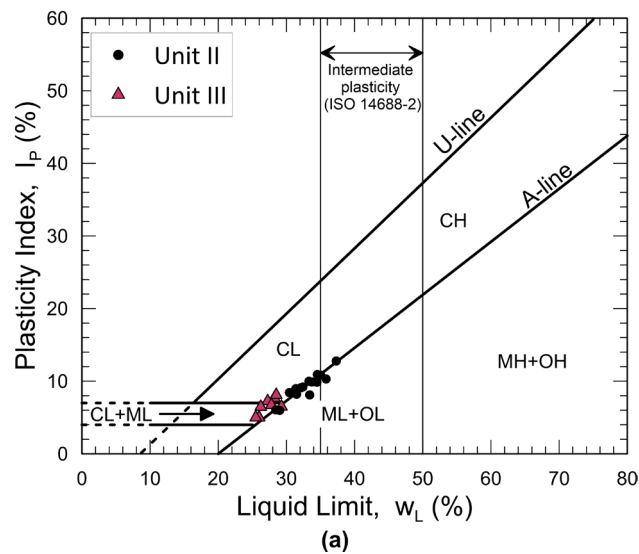


Figure 13. Casagrande plasticity chart with results of Atterberg limits on soil Unit II and III.

5.2 Total unit weight and void ratio

Total unit weights (γ_t) are estimated from the Multi Sensor Core Logger (MSCL), from direct measurement of advanced laboratory test specimens and from measured specimen water contents. The MSCL measures soil density based on emitted gamma ray attenuation using a ^{137}Cs radioactive source and a sodium iodide, NaI (TI) radiation detector. Figure 7c shows that the total unit weight in Unit II generally falls between 18.9 kN/m^3 and 19.2 kN/m^3 . In Unit III the total unit weight increases with depth from about 19.5 kN/m^3 at 12 m to about 20.5 kN/m^3 at 15 m, with an average value of 19.9 kN/m^3 . Results from the MSCL show an increase in total unit weight in Unit II. The trend is similar to that obtained from laboratory results based on direct measurements and water contents. However, the MSCL results are slightly higher. This may be due to whole core measurements where total density measurements integrate the entire sample thickness.

From a constant specific gravity of 2.69 (see section 5.3) the calculated in situ void ratio (e_0) decreases from about 0.82 at 5 m depth, to 0.6 at 15 m.

5.3 Unit weight of solid particles

Measured unit weight of solid particles (γ_s) ranges between 26.1 kN/m^3 and 26.5 kN/m^3 , with an average value of 26.3 kN/m^3 (specific gravity, $G_s=2.69$), see Figure 12.

6 Engineering properties

A number of in situ and advanced laboratory tests were performed to determine the engineering properties of the silt units at Halden (see Table 1 for the general test procedures). In this section the measured in situ data are first presented, followed by a comparison of engineering properties from laboratory test results and the derived parameters from in situ test results. The results focus on the silt units (Units II and III).

6.1 In situ testing measurements

6.1.1 Field vane testing

Field vane testing (FVT) was performed using a Geotech AB 130 × 65 mm vane with a tapered lower end in general accordance with the Norwegian guidelines [20]. After pre-drilling down to about 4.5 m the vane was advanced to the target depth from the ground level encased in a protective housing. The vane was then pushed out of the housing and rotated using electric heads and the torque was measured on the drill rig. Both intact and remolded tests were conducted at a rate of shearing of about 0.1 °/s. Remolded tests were performed after 10 full revolutions of the vane. The intact and remolded FVT results are presented in subsequent Sections 6.8 and 6.13, respectively.

6.1.2 Cone penetration testing

A number of different manufacturers' piezocones were tested at Halden, including Geomil, A.P.van den Berg, Pagani, Environmental Mechanics (Envi) and Geotech AB cones. They were all 10 cm² compression cones with 150 cm² friction sleeves and the pore pressure transducer located in the u_2 position. The CPTU tests were performed in general accordance with Norwegian guidelines [58] and ISO 22476-1 [16]. Figure 14a to Figure 14f present selected measured (corrected cone resistance, q_t , pore pressure, u_2 , and sleeve friction, f_s) and derived (normalized cone resistance, Q_t , pore pressure ratio, B_q , and soil behavior type index, I_c) CPTU parameters from a number of tests conducted across the test site. In the silt units, Units II and III, q_t typically plots around 1 MPa, similar to that of the clay unit below. In the deeper parts of the silt deposit q_t increases from 1 MPa at 12 m depth to about 2 MPa at around 16 m depth. Normalized cone resistance ($Q_t = [q_t - \sigma_{v0}]/\sigma'_{v0}$) is generally high in the top soil, but decreases to about 7.5 in the depth range 5–16 m. Excess pore pressures are generated behind the cones in the silt and clay units, and the pore pressure ratio, $B_q = (u_2 - u_0)/(q_t - \sigma_{v0})$, is generally around 0.1–0.3 in the silt units and 0.8–1.0 in the deeper clay. Previous experience on different soils [59] has shown there is some variability in the measured sleeve friction, f_s between the different cones tested at the site. The soil behavior type index, $I_c = [(3.47 - \log Q_t)^2 + (\log F_r + 1.22)^2]^{0.5}$, generally plots between 2.6 and 2.95 (Silt mixtures—clayey silt to silty clay). Normalized friction ratio, $F_r = 100\% \times f_s/(q_t - \sigma_{v0})$, ranges from 1% to 3% depending on cone manufacturer. As shown in Figure 15, normalized soil behavior type (SBT_N) charts [60] based on Q_t , F_r and B_q from CPTU location HALC11

typically indicate SBT zones 4 (Silt mixtures clayey silt to silty clay) and 5 (Sand mixtures silty sand to sandy silt).

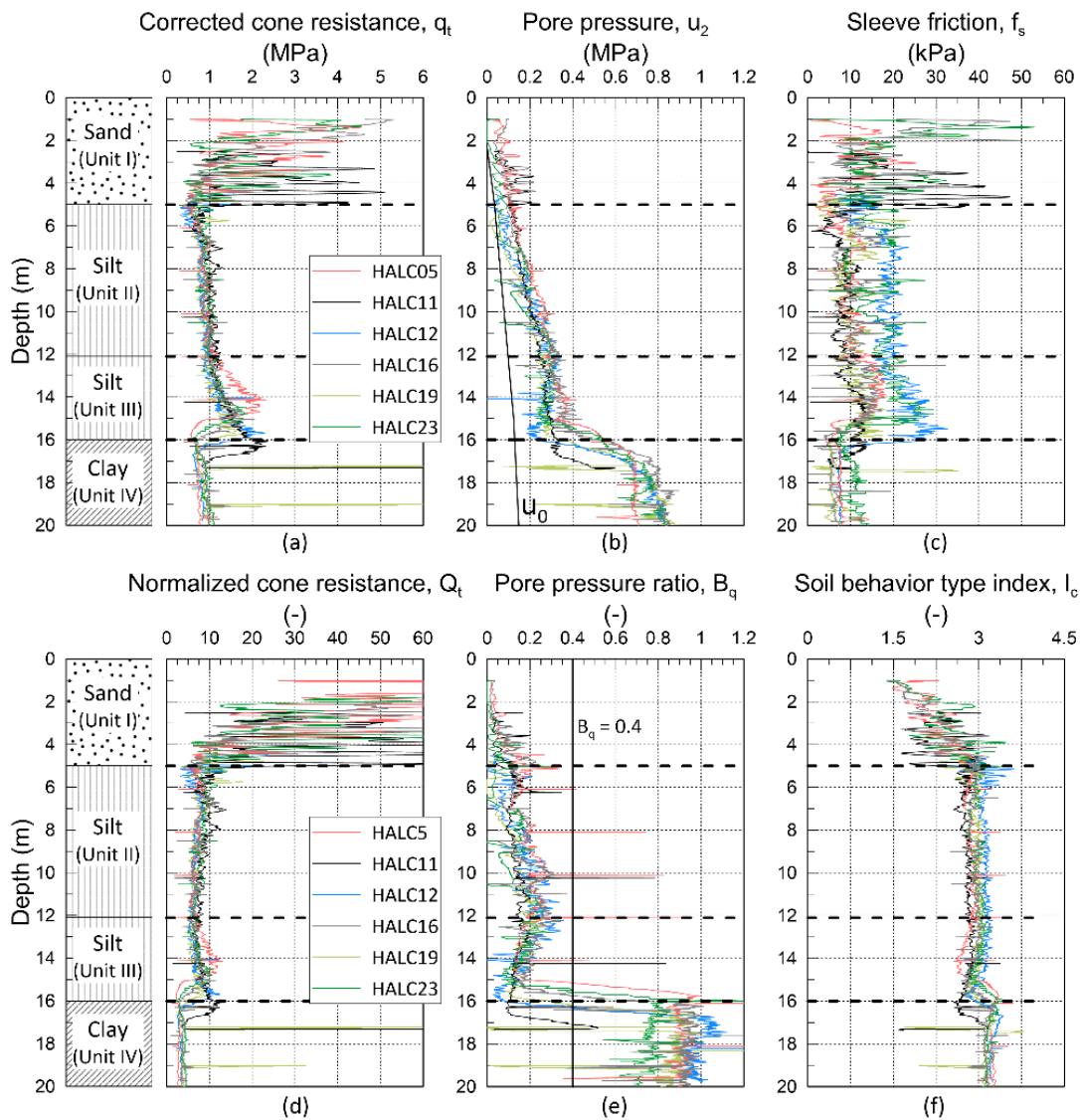


Figure 14. CPTU data from six locations; (a) cone resistance, q_c , (b) shoulder pore pressure, u_2 , (c) sleeve friction, f_s , and derived parameters (d) normalized cone resistance, Q_t , (e) pore pressure ratio, B_q , and (f) soil behavior type index, I_c .

6.1.3 Shear wave velocity

Direct measurements of shear wave velocity were made during a number of seismic cone penetration and seismic dilatometer tests at the site using a seismic add-on module with the original cone/dilatometer. Two multi-channel analyses of surface waves (MASW) profiles were also acquired. The SCPTU/SDMT configurations had a source at ground level and two geophones mounted behind the cone or dilatometer with a 0.5 or 1.0 m spacing thus giving a measure of shear wave velocity for a vertically propagating horizontally polarized shear wave, V_{vh} . In order to increase the signal-to-noise ratio and reduce the incoherent noise the seismic traces were typically stacked and filtered through a Butterworth bandpass filter. The velocity was computed from the time lag corresponding to the maximum of the cross-correlation between the two geophone signals. The MASW data acquisition was conducted using a linear array of 24 vertical geophones with a natural frequency of 4.5 Hz, and the inversion of the dispersion curves provided a 1D shear wave velocity, V_s , profile averaging the subsurface properties below the geophone array. Figure 16 demonstrates a clear trend of increasing shear wave velocity from about 110 m/s at 2 m depth to about 200 m/s at 16 m. The higher shear wave velocities at location HALC13 compared to the general trend from the other locations are likely associated with a higher uncertainty in the velocity estimates at this location (greater error estimates). There is generally a very good agreement between the SDMT and the SCPTU results. However, the MASW results (HALM01 and HALM02) are somewhat higher than the general trend from the other test methods. The inversion data fit was of limited quality, and as a result of the decreasing depth to bedrock along the geophone array the velocities below 8 m to 12 m depth likely integrate bedrock velocities and are removed. A MASW survey conducted by the University of Iceland demonstrated increased resolution compared to the tests at HALM01 and HALM02, and the results coincide better with the SCPT data below 8 m depth (see Figure 16).

6.1.4 Flat dilatometer testing

Measured flat dilatometer data from location HALD01 is presented in Figure 17a to Figure 17e. Testing was conducted in general accordance with ISO 22476-11 [17]. The corrected pressure readings, P_0 and P_1 , are presented along with the three intermediate DMT parameters I_D (material index), K_D (horizontal stress index), and E_D (dilatometer modulus), e.g. [61,62]. There is some scatter above 5 m. The data is more consistent in the silt and clay units below. Soil classification charts based on I_D and E_D , e.g. [62], typically classify the silts in Units II and III as mud, mud and/or peat or clay. Based primarily on I_D [62] the silts are identified as clays, but it is noted that; " *I_D sometimes misdescribes silt as clay and vice versa, and of course a mixture of clay-sand would generally be described by I_D as silt*". Assessment of OCR and K_0 using the Marchetti equations [61] are presented in Sections 6.2 and 6.3.

6.1.5 Self-boring pressuremeter testing

Four self-boring pressuremeter tests were conducted in location HALP01 in general accordance with ISO 22476-5 [18] using the Cambridge InSitu Ltd. six-arm pressuremeter probe. The borehole HALP01 was drilled using an auger bit with a nominal size of 120 mm using water flush. The SBPT was self-bored to the required depth with the cutter positions optimized and at a rate such that a minimum of disturbance was introduced in the soil. After the first three tests a steel casing was advanced to 11.5 m to stabilize the borehole. The probe was calibrated prior to and after testing and corrections for membrane stiffness were made upon data reduction. The four test results from 6.1 m, 8.0 m, 10.0 m and 12.0 m depth, plotted in Figure 18, are average data for each tier of strain arms. Three to four unload-reload loops were conducted at each depth.

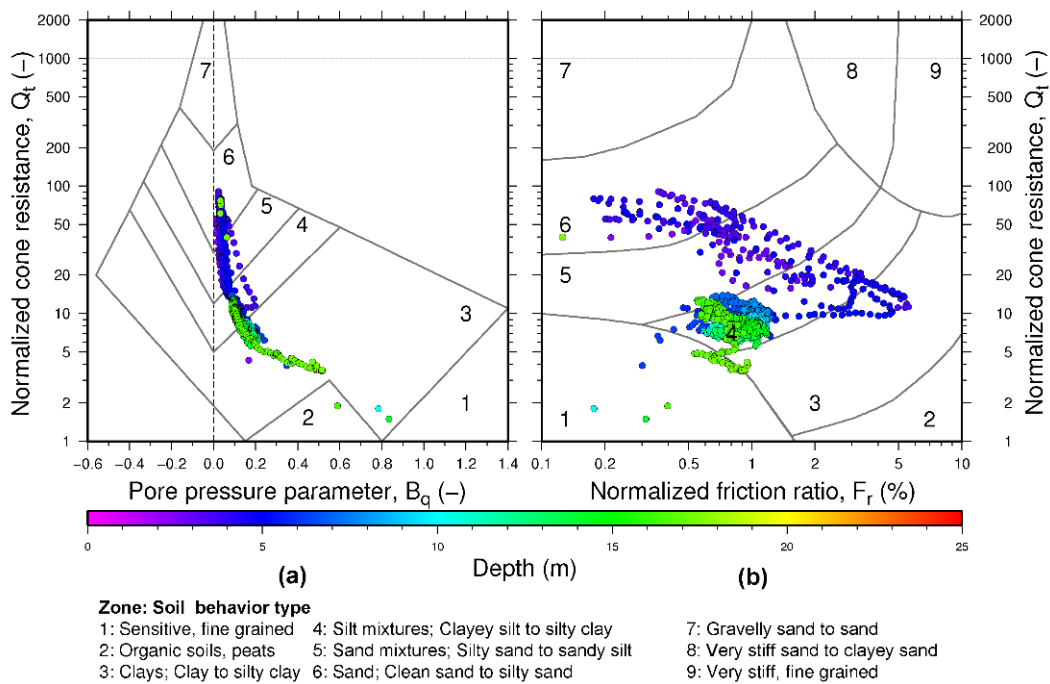


Figure 15. Soil behavior type charts [60] from location HALC11 by means of (a) normalized cone resistance, Q_t , versus pore pressure parameter, B_q , and (b) normalized cone resistance, Q_t , versus normalized friction ratio, F_r .

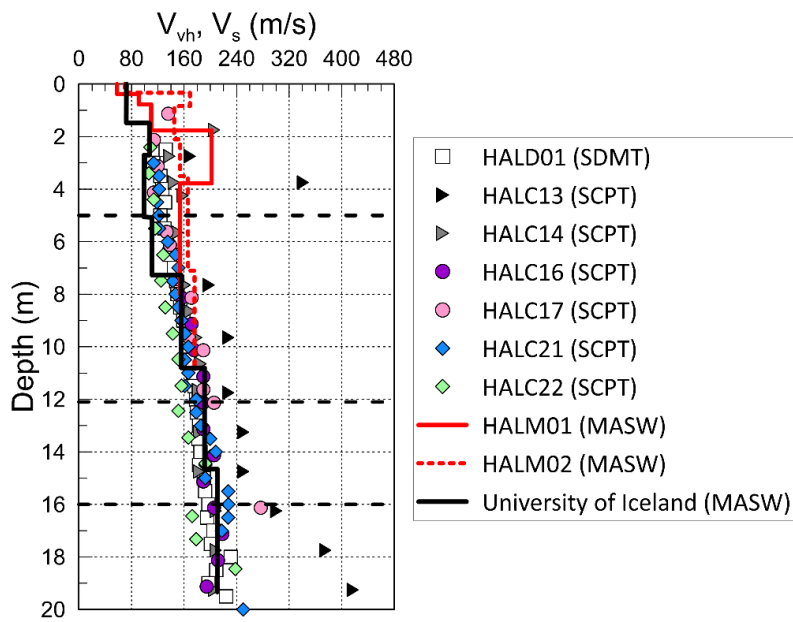


Figure 16. In-situ shear wave velocity (V_{vh} , V_s) from SCPT and SDMT, and Multichannel Analyses of Surface Waves (MASW).

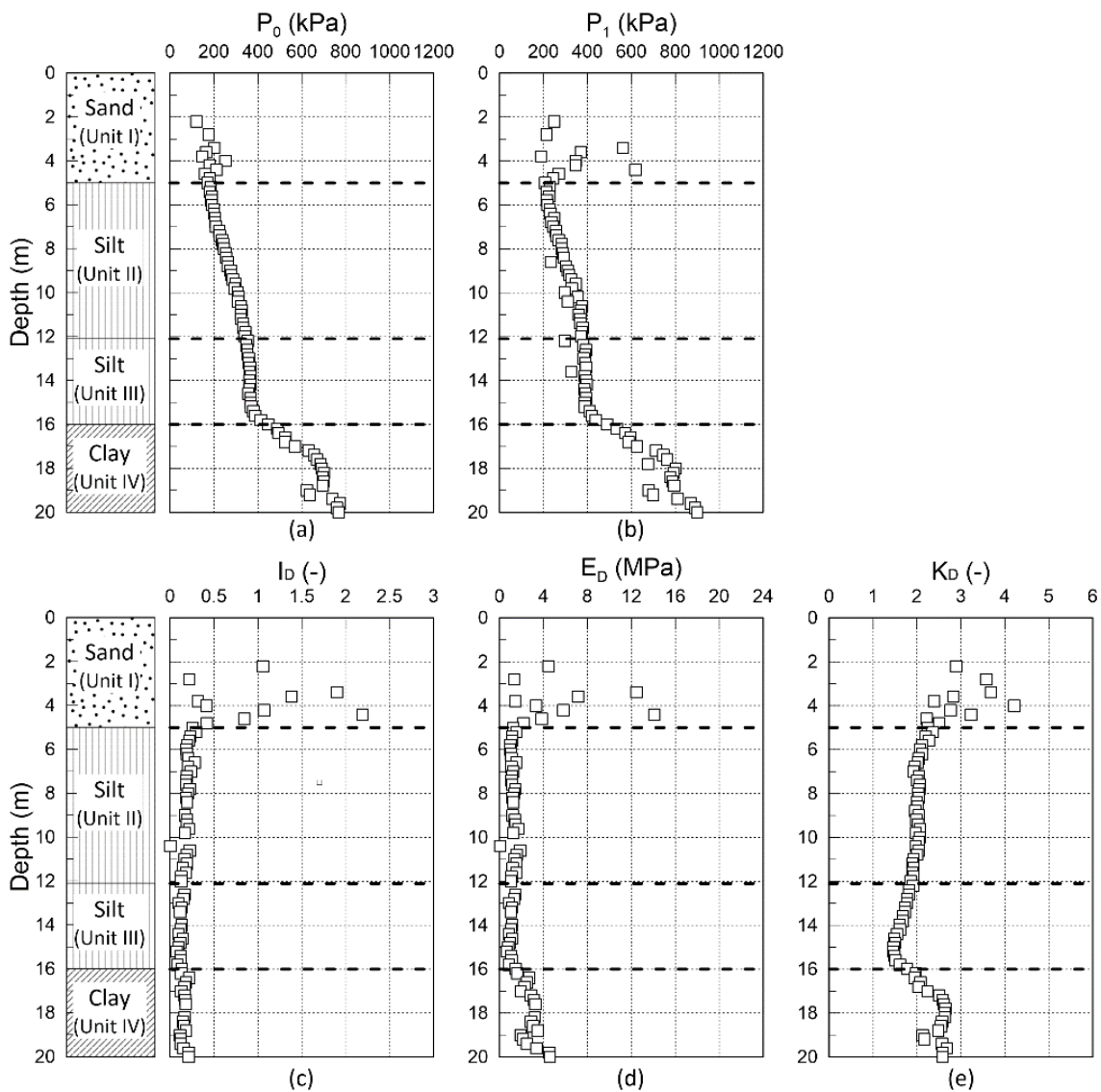


Figure 17. Results of DMT testing with (a) corrected first reading, (b) corrected second reading, and intermediate DMT parameters (c) material index, I_D , (d) horizontal stress index K_D , and (e) dilatometer modulus, E_D .

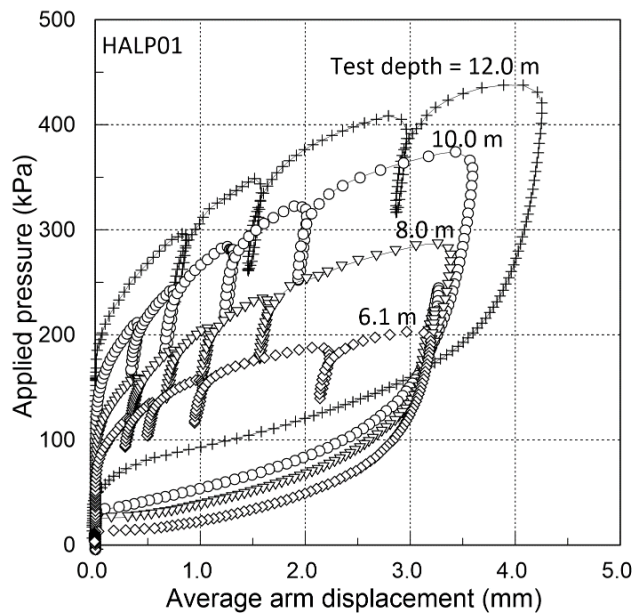


Figure 18. Typical self-boring pressure meter results. Interpretation of σ_{h0} and $S_{u,SBP}$ based on Marsland and Randolph methodology [63].

6.2 Overconsolidation ratio, OCR

An evaluation of the overconsolidation ratio (OCR) profile is dependent on reliable interpretation of the preconsolidation stress or yield stress, σ'_p , from laboratory oedometer tests or an appropriate correlation of yield stress to cone resistance, none of which yet exist for silts. As will be discussed in Section 6.5 the Halden silt 1D compression curves of log effective vertical stress with void ratio are generally very flat, and interpretation of σ'_p from these oedometer tests have proved very challenging. Both the conventional Casagrande interpretation [64], Janbu [65] and Pacheco Silva [66] methods resulted in unreliable values of σ'_p . However, the geological history of the area (see Section 3) is well understood and no loading or large erosion events are likely to have caused overconsolidation of the soil units at the research site. The well-established correlations of yield stress to CPTU cone resistance valid for natural clays [67], $\sigma'_p = k \times (q_t - \sigma_{v0})$ suggests a normally consolidated stress history for the clay (Unit IV) below the silt Units II and III (see Figure 19a and Figure 19b). In this equation, k is a constant and in this case taken as 0.3, which is a typical value used for clays [68]. Normally consolidated or lightly overconsolidated clay (OCR= 1.0–1.3) at this depth is confirmed by the FVTs conducted at the site using the Chandler methodology [69], where $\sigma'_p = \sigma'_{v0} \times [(S_{u,FVT}/\sigma'_{v0})/S_{FVT}]^{1.05}$ and S_{FVT} is estimated as a function of plasticity index (in this case taken as 0.15 and 0.2 in the silt and clay units, respectively, based on assumed plasticity indices, $I_p = 10\%$ and 20%). From the geological history and evidence of the near normally consolidated stress state of the lower clay one can thus infer that the uniform silt Units II and III above this clay unit, are also normally consolidated. This implies that the CPTU and FVT correlations discussed above, which suggest OCR in the range of 2

to 5 in the silt Units II and III, are unreliable and inappropriate for this soil type. Any light overconsolidation is likely an effect of aging and fluctuating ground water table. Yield stress and OCR interpreted from DMTs (Figure 19a and Figure 19b) using the horizontal stress index, K_D [61] (valid for clays with $I_D < 1.2$) suggest $OCR \leq 1$ and $OCR = 1.5$ in the silt and clay units, respectively. Dilatometer tests were used to confirm a low to medium overconsolidation ratio ($OCR = 1.2\text{--}3.7$) in the silt layers of the Malamocco test site, near Venice, Italy [7]. Based on the above discussion an OCR in the range of 1.0 to 1.3 at Halden is considered reasonable. Following from this OCR assessment a k-factor of 0.15–0.2 would be more appropriate in the Halden silt, i.e. $\sigma'_p = 0.2 \times (q_t - \sigma_{v0})$.

6.3 Coefficient of earth pressure at rest, K_0

Coefficient of earth pressure at rest, $K_0 = \sigma'_{h0}/\sigma'_{v0}$ (Figure 19c.), was derived from DMT results using the clay correlation to K_D [61], and from nine anisotropically consolidated drained and undrained triaxial tests in compression loading (CADC, CAUC) using the expression [70]:

$$K_0 = (1 - \sin \phi'_{cv})OCR^{\sin \phi'_{cv}} \quad (1)$$

where, ϕ'_{cv} is the constant-volume effective stress friction angle for triaxial compression [70], in this case assumed to be equal to ϕ'_{mo} obtained in the CADC and CAUC tests at maximum obliquity, $(\sigma'_1/\sigma'_3)_{max}$. In this expression an OCR of 1.3 has been assumed (see Section 6.2).

Moreover, in situ horizontal total stresses were assessed from the four SBPTs plotted in Figure 18 based on a methodology proposed for London clay by Marsland and Randolph [63]. In this approach, the total horizontal stress and undrained shear strength of the soil adjacent to the probe are estimated by iteration. Once a first qualified value of σ_{h0} is assumed, the apparent mobilized cavity shear stress at the pressuremeter boundary can be derived from the measured expansion curve following the Palmer analyses [71]. The peak shear strength of the soil is estimated from the maximum slope of the P-ln ($\Delta V/V$) curve, where P is the measured pressure, ΔV is the increase in volume from the reference state, and V is the current volume of the measuring cell at the measured pressure. The point at which the pressure-deformation curve becomes significantly non-linear should correspond the in situ horizontal total stress plus the undrained shear strength in clays ($\sigma_{h0} + s_{u,SBP}$). The methodology assumes fully undrained conditions. However, as noted by Wroth [72], the stress and strain fields surrounding the pressuremeter do not remain homogeneous during membrane expansion, and partial drainage will occur even in clays. As such, interpretation of SBPTs in silts is challenging and somewhat uncertain. K_0 interpreted from the four tests at Halden (Figure 19c) are consistently higher than the values interpreted from laboratory triaxial tests. This could indicate an over prediction of the effective horizontal stress resulting from partial drainage effects.

Despite uncertainties associated with the clay-based interpretation of the SBPT and DMT data there is fair agreement between the in situ and laboratory test results, and K_0 generally ranges between 0.6 and 0.45.

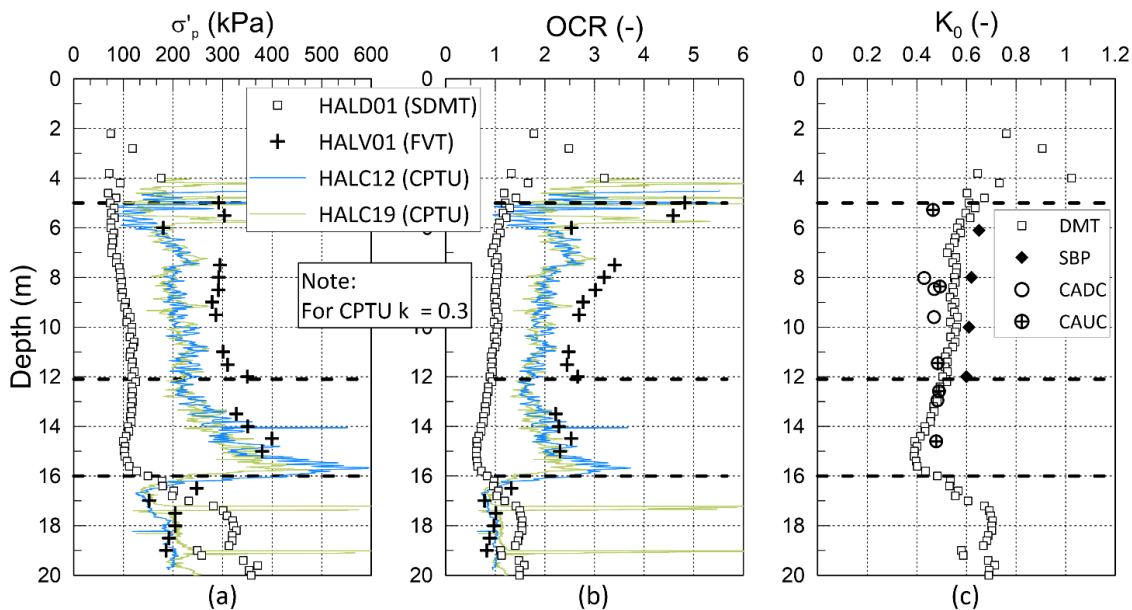


Figure 19. Stress history data from field and laboratory testing. (a) yield stress, σ'_p , (b) overconsolidation ratio, OCR, and (c) coefficient of earth pressure at rest, K_0 .

6.4 Small strain shear modulus

Small strain shear modulus, G_{max} , is interpreted from a number of SCPTs, one SDMT and two MASW profiles. Figure 20 presents G_{max} computed from in situ shear wave velocity measurements depicted in the previous Figure 16. Generally, the SCPT and SDMT G_{max} results increase linearly from about 30 MPa at 5 m depth to about 75 MPa at 16 m depth. Two SCPT results from location HALC13 plot outside the scale and are indicated in the figure ($G_{max} = 287$ mPa and 354 MPa). However, the results from this location are generally high, and likely a result of greater uncertainty in the shear wave velocity estimates (see Section 6.1.3). The linear increase in V_{vh} in the silt units is very consistent with the Rix and Stokoe correlation of G_{max} to cone resistance for sands [73], presented in the figure. G_{max} computed from the Mayne and Rix correlation of shear wave velocity to corrected cone resistance [74], valid for natural clays, plot below the in situ and MASW results. Bender element (BE) tests [44], performed on triaxial specimens (at $\sigma'_{vc} = \sigma'_{v0}$, $\sigma'_{hc} = \sigma'_{h0}$) and DSS specimens (at $\sigma'_{vc} = \sigma'_{v0}$), indicate that the small strain shear modulus measured in the laboratory is generally lower than the in situ test results.

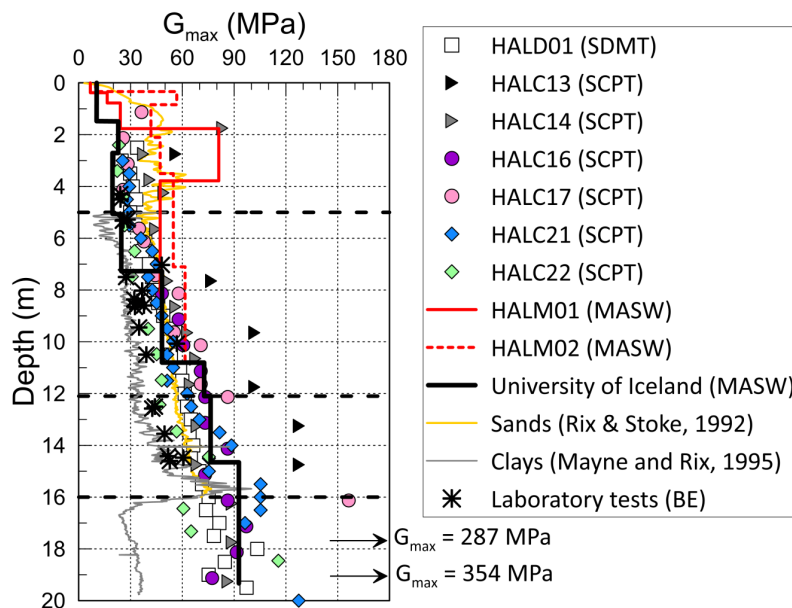


Figure 20. Small strain shear modulus, G_{max} , from field and laboratory measurements of V_{vh} and V_s (SCPT, SDMT, MASW and bender elements).

6.5 Constrained modulus

For soft clays, primary consolidation properties are normally interpreted from oedometer curves of log effective stress (σ'_v) with strain (ϵ_v) or void ratio (e). Creep properties from plots of ϵ_v or void ratio with log time. This approach may be inappropriate for silts and other intermediate soils leading to unreliable interpretations, while, Janbu's theory for primary and secondary settlements [75] may be more suitable. In Janbu's framework the stress induced primary consolidation is calculated with an effective stress dependent constrained modulus ($M = \Delta\sigma'_v/\Delta\epsilon_v$). As observed in oedometer tests on other silts, e.g. [7,76], the three typical Halden CRS oedometer curves (rate of strain 5%/hr) of log effective stress with void ratio are generally quite flat (see Figure 21a). The compression curves are presented in linear scale in Figure 21b, which show no distinct yield as typically displayed by structured clays. As such interpretation of σ'_p from these curves is considered misleading. This 1D compression behavior seems to be characteristic of some intermediate soils [76–79]. Janbu's modulus framework for silts ($M = 1/m_v = m \times p_a \times [\sigma'_v/p_a]^{1-a}$, where m_v is the volume compressibility $\Delta\epsilon_v/\Delta\sigma_v$, m is the modulus number, p_a is the reference stress = 100 kPa, and a is a stress exponent) gives a reasonable fit, as demonstrated in Figure 21d when the modulus number $m = 75$ and stress exponent $a = 0.25$ are taken. The Janbu modulus framework for clays ($M = m \times \sigma'_v$) is presented in the same figure using $m = 30$, but does not provide a good fit. Janbu's silt model has also been applied on Icelandic silts [80], on Irish silts [78] and on another Norwegian silt from Os [79].

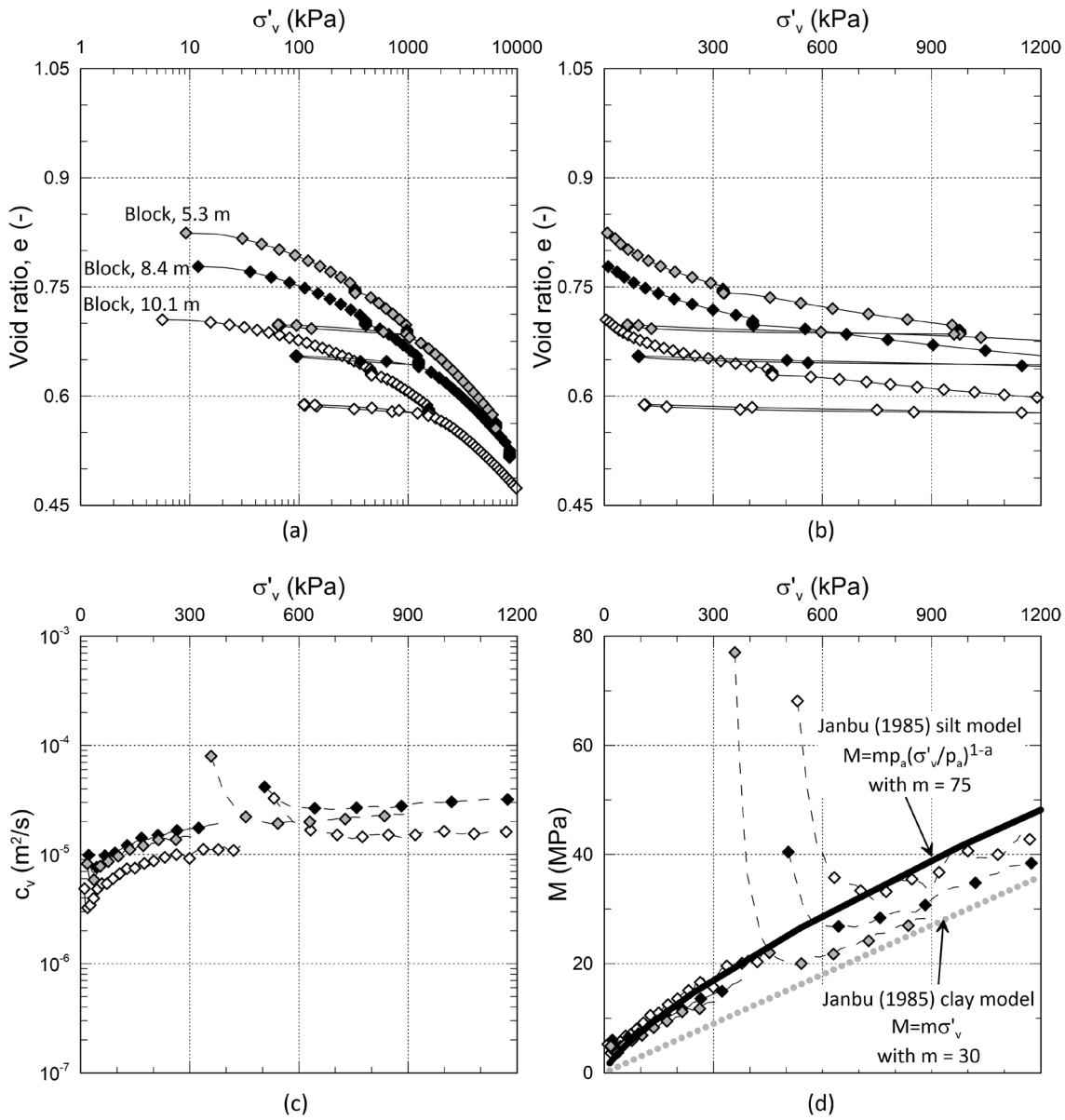


Figure 21. Three typical results from CRS testing on specimens from Halden block samples. (a) Void ratio versus log vertical stress, (b) void ratio versus vertical stress, (c) coefficient of consolidation, c_v , versus vertical stress, and (d) constrained modulus, M versus vertical stress.

Values of the constrained modulus at the in situ effective vertical stress, M_0 , from CRS and IL tests on specimens from block samples (HALB04) are plotted with depth in Figure 22a. With one exception at about 15 m depth, M_0 ranges from 5 to 10 MPa. This is consistent with the CPTU results from locations HALC11 and HALC12 using the correlation $M_0 = \alpha_i \times q_{net}$ with $\alpha_i = 10$ [67] and Janbu's modulus framework for silts using $m = 70\text{--}80$, also presented in the figure.

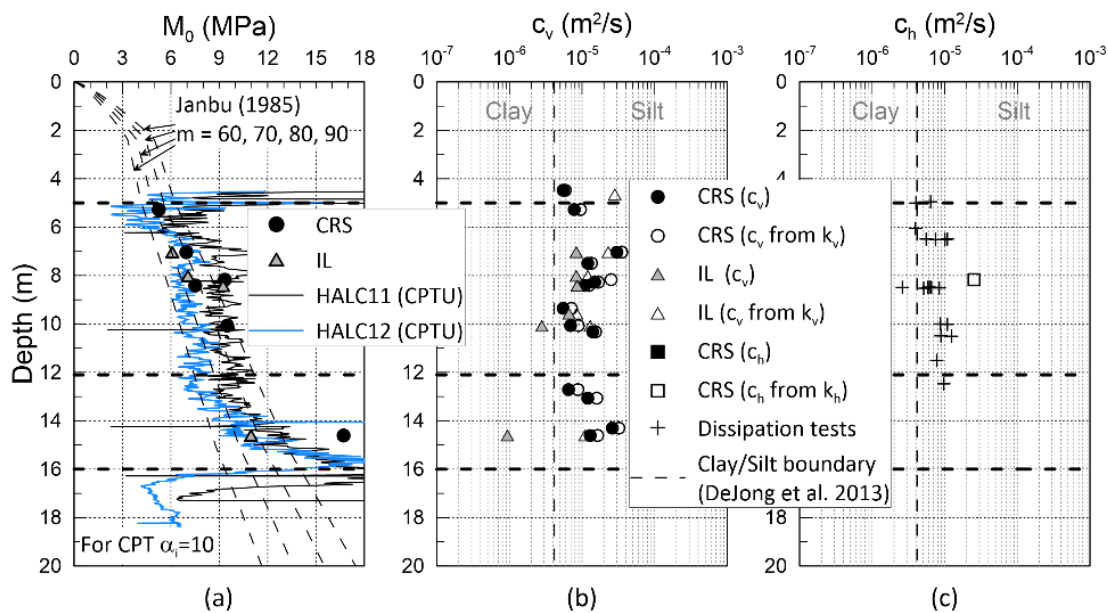


Figure 22. (a) Constrained modulus at the in situ effective vertical stress, M_0 and (b) vertical and (c) horizontal coefficient of consolidation with depth, with DeJong et al. [81] clay-silt transition indicated

6.6 Coefficients of consolidation

Coefficient of vertical consolidation (c_v) with log effective stress from three typical Halden CRS oedometer tests are presented in Figure 21c. c_v at the in situ vertical effective stress is determined from the base pore pressure (u_b) in CRS oedometer tests [36], and from IL oedometer tests using the root time fitting method [82]. The results are consistent with the values of c_v computed from the direct measurement of vertical hydraulic conductivity (k_v , see Section 6.7 and [36]) using the relationship $c_v = k_v / (m_v \times \gamma_w)$. In this equation m_v is the volume compressibility and γ_w is the unit weight of water at 20 °C. The results plotted in Figure 22b suggests an average coefficient of vertical consolidation of $1.3 \times 10^{-5} \text{ m}^2/\text{s}$, or about 400 m^2/year . Results from other silts are typically in the order of 10 to 350 m^2/year [78,83,84].

Coefficient of horizontal consolidation (c_h) is interpreted from a number of CPTU dissipation tests [85], where t_{50} is determined from the square root method [86], and determined in the laboratory on a block sample test specimen mounted horizontally in the CRS oedometer cell. All dissipation tests were conducted after penetrating the piezocones to target depth using standard CPTU penetration rate of 20 mm/s. Figure 22c shows that the in situ results indicate slightly lower c_h compared to the c_v determined in CRS and IL oedometers. However, the differences are not significant and the c_h result determined in the laboratory confirms this. Further, during dissipation testing, Halden silt exhibited a non-standard (dilatatory type) behavior which introduces uncertainties in the interpretation of t_{50} and c_h , since the applied methods were generally developed for clays, and do not consider partial drainage.

6.7 Hydraulic conductivity

Constant-head hydraulic conductivity tests were conducted at different stress levels during a selected number of oedometer tests and during the consolidation stage of a number of triaxial tests. Hydraulic conductivity was determined by flowing de-aired water through the specimens, from bottom to top, by a 100 mm mercury column in a U-shaped saran tubing. The amount of water flowing in and out of the specimen was measured separately, and the tests were continued until the water inflow and outflow were approximately equal [36]. Both vertical and horizontal hydraulic conductivity (k_v , k_h) are presented in Figure 23. Values from oedometer test specimens represent the hydraulic conductivity at zero axial strain (back-extrapolated along the linear e-log k line [36]), i.e. at a void ratio near in situ conditions. Values from triaxial test specimens represent the hydraulic conductivity near the in situ effective stress state (σ'_{vc} , σ'_{hc}), i.e. after consolidation and some subsequent change in void ratio (Δe) has occurred. Due to the larger volume of soil and the greater height of the triaxial test specimen the hydraulic conductivity measurements made on these specimens are generally considered more reliable. The average k_v of the triaxial test specimens is 9.8×10^{-9} m/s.

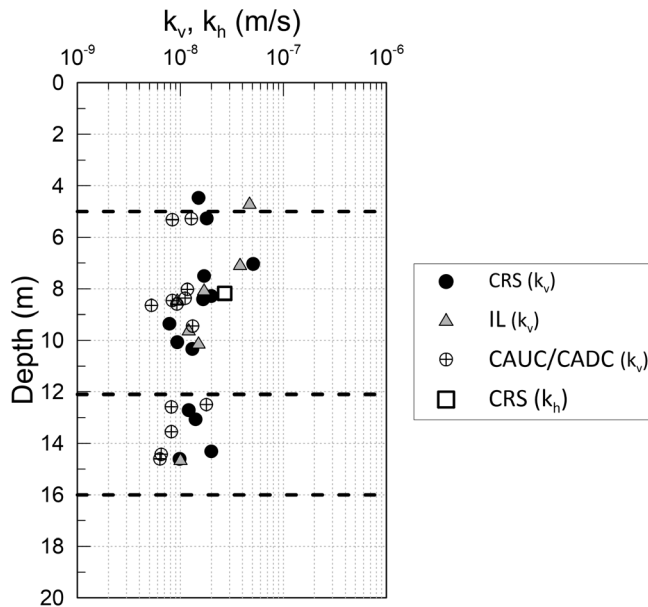


Figure 23. Hydraulic conductivity (k_v , k_h) from laboratory testing.

6.8 In situ undrained shear strength—field vane testing

Drainage conditions in silts during shear depend on a number of factors, including but not limited to loading regime, drainage path, clay content etc. An effective stress approach may in some cases be a more valid approach for silts and silty soils, but the total stress approach is often used in engineering practice and when an evaluation of the undrained shear strength is required. The field vane test results plotted in Figure 24a show that the interpreted peak intact undrained shear strength in the silt units is fairly constant with depth at around 40–45 kPa, except for some higher values close to the silt-clay interface around 14–16 m depth. No empirical correction factors have been applied. As will be discussed in subsequent sections, the results are very consistent with the derived undrained shear strength from location HALC12 using an undrained CPTU interpretation with $N_{kt} = 18$, and generally plot between the $s_u = 0.3\sigma'_{v0}$ and $0.5\sigma'_{v0}$ lines, indicated in the figure. As observed in the Norwegian Os silt [79] and the Swedish Borlänge silt [87] field vane test results in silt are typically significantly lower than the results from undrained triaxial tests on the same material, when s_{uc} is interpreted at simple peak or 10% axial strain like for clays. The reason for the high triaxial strength is the strong tendency for dilatant behavior during undrained shear (see Section 6.12). It should be noted, however, that field vane testing in silt may be subject to drained or partially drained conditions. As noted by Chandler [69], if the coefficient of consolidation is not sufficiently low with respect to the rate of vane rotation, consolidation may occur. Moreover, Blight [88] developed an approximate theory, supported by experimental tests in a silt (tailings, 5–15% clay content, $c_v = 370 \text{ m}^2/\text{year}$), by which one may determine the rate of vane rotation required to ensure undrained conditions. Based on these theoretical drainage curves for the vane test [69], indications

are that the conventional rate of rotation (6–12°/min) does not provide shearing under fully undrained conditions in the silt units at Halden. Thus, the vane results between 5 m and 16 m depth in Figure 24a may not be an accurate measure of the undrained shear strength.

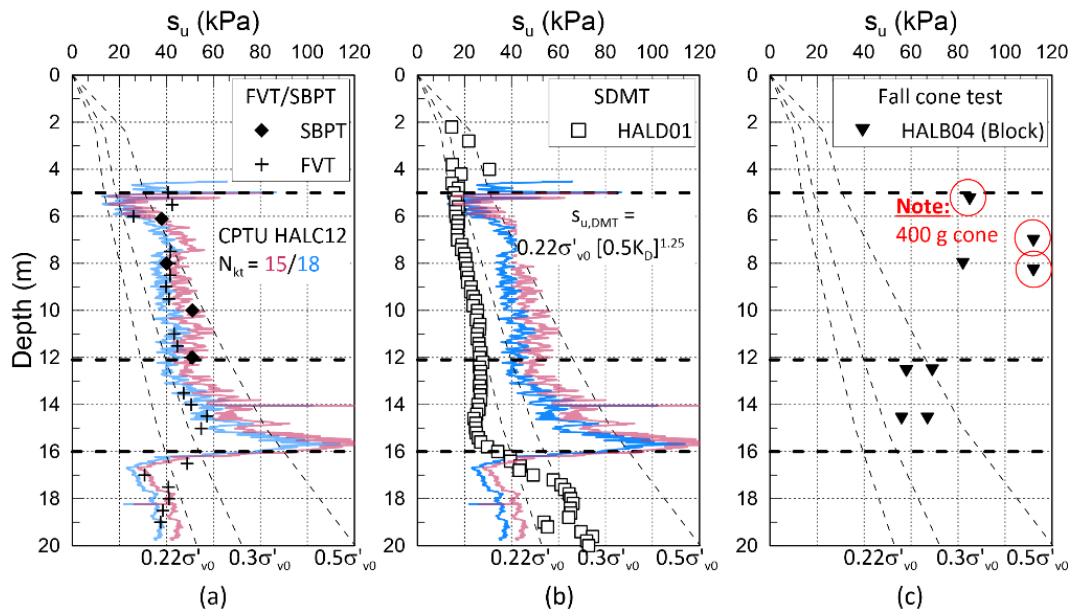


Figure 24. Undrained shear strength from (a) field vane tests, self-boring pressuremeter tests and CPTU, (b) DMT and CPTU, (c) fall cone tests.

6.9 In situ undrained shear strength—pressuremeter testing

Figure 24a presents undrained shear strengths from the four self-boring pressuremeter tests interpreted using the Marsland and Randolph approach [63], see also Section 6.3. In this approach, undrained conditions are assumed, and the total horizontal stress (σ_{h0}) and peak cavity shear stress ($s_{u,SBP}$) at the pressuremeter boundary are estimated by iteration. The point at which the pressure-deformation curve becomes significantly non-linear should correspond to the in situ horizontal total stress plus the undrained shear strength in clays. The undrained shear strengths estimated from this approach are consistent with field vane results, and $s_{u,SBP}$ ranges from 38 kPa to 51 kPa. Assessment of undrained shear strength using the limit pressure (p_L) [63] yields values in the range of 31 kPa to 68 kPa but are associated with very large strains. A third interpretation approach, the Gibson and Anderson approach [89], is based on the assumption of an elastic-perfectly plastic material and yields significantly larger $s_{u,SBP}$ values. In clays, over predictions of undrained shear strength from SBPTs compared to laboratory tests on undisturbed soil have been observed [72,90]. This is typically explained by partial consolidation during expansion (high gradients of pore pressure in the radial direction) and strain rate effects (increased “viscosity”—shearing at strain rates much faster than

conventional laboratory tests yields larger undrained shear strength). Noting that the SBPT is a rather slow test compared to other in situ techniques, e.g. the CPTU, partial drainage may have prevailed during membrane expansion at Halden. As a result, there is some uncertainty associated with the $s_{u,SBP}$ results in Figure 24a. The fact that the interpreted undrained shear strength values show fair agreement with the field vane test results and the CPTU correlation to q_t could be a result of compensating effects in the measurements and interpretation, and as such, somewhat fortuitous.

6.10 In situ undrained shear strength—flat dilatometer testing

DMT results in Figure 24b show that the Marchetti correlation for undrained shear strength from DMT [61], $s_{u,DMT} = 0.22 \times \sigma'_{v0} \times (0.5K_D)^{1.25}$ has been found to fall somewhere close to the average undrained shear strength profile in some clays. It appears that at Halden the correlation provides estimates on the low side of both field vane, pressuremeter and CPTU results evaluated with $N_{kt} = 15$ –18. This is explained by the fact that the horizontal stress index, K_D is about 2 in the silt layers, and this corresponds to an interpreted OCR of 1. As a result between 5 m and 13 m the undrained shear strength interpreted from DMT fall close to the normally consolidated line ($0.22\sigma'_{v0}$), also indicated on the plot. For Halden silt, $s_{u,DMT} = 0.45 \times \sigma'_{v0} \times (0.5K_D)^{1.25}$ would provide a better fit with the FVT data.

6.11 In situ strength—cone penetration testing

Undrained shear strength from the Halden CPTU data was estimated using $s_u = (q_t - \sigma_{v0})/N_{kt}$, with cone factors N_{kt} of 15–18 (see Figure 24a and Figure 24b). While the N_{kt} for assessment of shear strength from undrained triaxial tests in compression (s_{uC} interpreted at the maximum excess pore pressure, u_{max}) is about 15, the N_{kt} factor for field vane strength is closer to 18. These differences are attributed to the different mode of shear between the two test methods, strain rate differences, choice of failure criteria and possible partial drainage in the field vane tests. As will be discussed in more detail in Section 6.12, the triaxial test specimens exhibit dilative behavior during undrained shear and, unlike the field vane results, do not exhibit a unique (peak) undrained shear strength. The derived $N_{kt} = 15$ for triaxial tests is fairly consistent with the B_q - N_{kt} relationship suggested by Lunne et al. [67] for several Norwegian clays, although the Halden N_{kt} values are somewhat on the low side of what could be expected from a soil with such low B_q values (typically, $B_q = 0.1$ – 0.25) [85]. But again, this is based on the reference CAUC s_{uC} taken at u_{max} which is the lowest derived value of s_u as discussed further in Section 6.12. Norwegian silts from the Brage offshore oil field (6%–15% clay size particles, $I_p = 8\%$ – 9%) and an onshore site in Stjørdal (0%–24% clay size particles) show N_{kt} values ranging from 15 to 30, according to Senneset et al. [91]. However, they point out that for soils with $B_q < 0.4$ a correlation between s_u and CPTU testing may be inappropriate due to partial drainage during penetration. Further, N_{kt} factors of 18 and 11 have been suggested for two Irish silts (5%–6% clay size particles, $I_p = 3\%$ – 17%) [78], and the Norwegian Os silt (3%–12% clay size particles, $I_p = 12\%$) [79],

respectively. In sum, when calibrated in reference to CAUC test results that exhibit dilative behavior, the resulting N_{kt} values depend significantly on what criterion is used to select s_{uC} as discussed below.

6.12 Undrained strength from laboratory testing

Index undrained shear strength by means of the fall cone tests (FC) were conducted in general accordance with the Norwegian standard [33], using a 100 g fall cone and in some cases a 400 g cone with both having a 30° cone angle. Results from a selected number of tests on block samples are presented in Figure 24c. Results from other boreholes are not presented to reduce factors related to; (i) variation in sampling technique, e.g. [76,79] while factors relating to (ii) fall cone operator dependency, (iii) scale effects, and (iv) local pockets of silt, sand or clay are other possible effects on the results. Three of the four shallow fall cone results in Figure 24c were obtained using a 400 g cone and all four tests yield strengths significantly higher than the triaxial (CAUC) test results determined at the u_{max} criterion, discussed below.

Anisotropically consolidated undrained triaxial tests (CAUC) and direct simple shear (DSS) tests were performed to investigate the behavior of the Halden silt under static undrained loading. Triaxial test specimens were trimmed from block samples, consolidated to the best estimate in situ stress conditions ($\sigma'_{vc} = \sigma'_{v0}$, $\sigma'_{hc} = \sigma'_{h0}$, with an assumed $K_0 = 0.5$; Section 6.3). Specimens were sheared at a nominal axial strain rate of 1.4 %/hour [40]. The DSS tests were conducted as constant volume tests in a Geonor DSS device using 35 cm² specimen area and wire reinforced membranes. Specimens were loaded directly to the best estimate in situ vertical effective stress ($\sigma'_{vc} = \sigma'_{v0}$) and sheared at a nominal shear strain rate of 5 %/hour [42]. The three selected triaxial test results in Figure 25a to Figure 25c show that, except for an initial contraction, the specimens show a strong tendency towards dilative behavior (i.e. strain hardening) upon shearing. Due to this behavior the interpretation of the undrained shear strength is complex and test results provide no unique (peak) undrained shear strength. The undrained shear strength from CAUC and DSS tests, depicted with an interpretation of CPTU HALC12 using $N_{kt} = 15$ and 18 in Figure 26a to Figure 26c, are determined using three different strength criteria [92];

- (a) $s_u = q_f$ at the maximum pore pressure, u_{max} ,
- (b) $s_u = q_f$ at the point of which the pore pressure parameter $A = (\Delta u - \Delta \sigma_3) / (\Delta \sigma_1 - \Delta \sigma_3) = 0$, i.e., equal to the drained shear strength for a CADC loading stress path,
- (c) $s_u = q_f$ at a limiting strain, γ_{lim} (an axial strain $\varepsilon_f = 5\%$, or $\gamma_f = 7.5\%$ in triaxial tests and at a shear strain $\gamma_{h,f} = 5\%$ in DSS).

Criterion (a) provides the lowest estimate undrained shear strength as the shear stress at this point is below the failure envelope and has not been fully mobilized, but together with criterion (b) is the most consistent interpretation procedure. While criterion (a) plots between the $s_{uC} = 0.3$ to $0.5\sigma'_{v0}$ lines, criteria (b) and (c) provide undrained shear strengths that plot much higher, and more scattered in the case of criterion (c). Two CAUC results from criterion (c) plot outside the scale in Figure 26c and are indicated in the figure ($s_{uC} = 131$ kPa and 177 kPa).

Typical DSS strength anisotropy ratios, $(s_{uD}/\sigma'_{v0}) / (s_{uC}/\sigma'_{v0})$ assessed at u_{max} , range from 0.70 – 0.78, with an average value of 0.74.

6.13 Remolded undrained shear strength and sensitivity

Remolded undrained shear strengths were determined from laboratory fall cone tests on block samples and field vane tests (Figure 27a). The remolded FVTs were conducted after 10 full revolutions of the vane and show that the remolded undrained shear strength is generally around 8 kPa. Fall cone results are somewhat more scattered, particularly in Unit II. Compared to the sleeve friction from two typical CPTU locations (HALC11 and HALC19) the field vane results agree very well. However, as discussed in Section 6.1.2 there is some variability in the measured sleeve friction between the different cones tested at the site. It should be noted that in Unit II and III the cone sleeve in location HALC12 recorded friction values twice the values recorded in HALC11 and HALC19.

Generally, soil sensitivity measurements from fall cone and field vane tests range between 2 and 7 (Figure 27b). The FVT results are somewhat more consistent with depth than the fall cone, and typically decrease from about $S_t = 7$ at 5 m depth to about $S_t = 5$ at 15 m. The sensitivity of the clay unit below 16 m depth plots around $S_t = 3$. Some studies have suggested that the field vane data should be used with caution as measured strength, particularly remolded values, may be high [79]. Furthermore, remolding can change the coefficient of consolidation of the soil and thus potential partial drainage effects may differ between the intact and remolded tests.

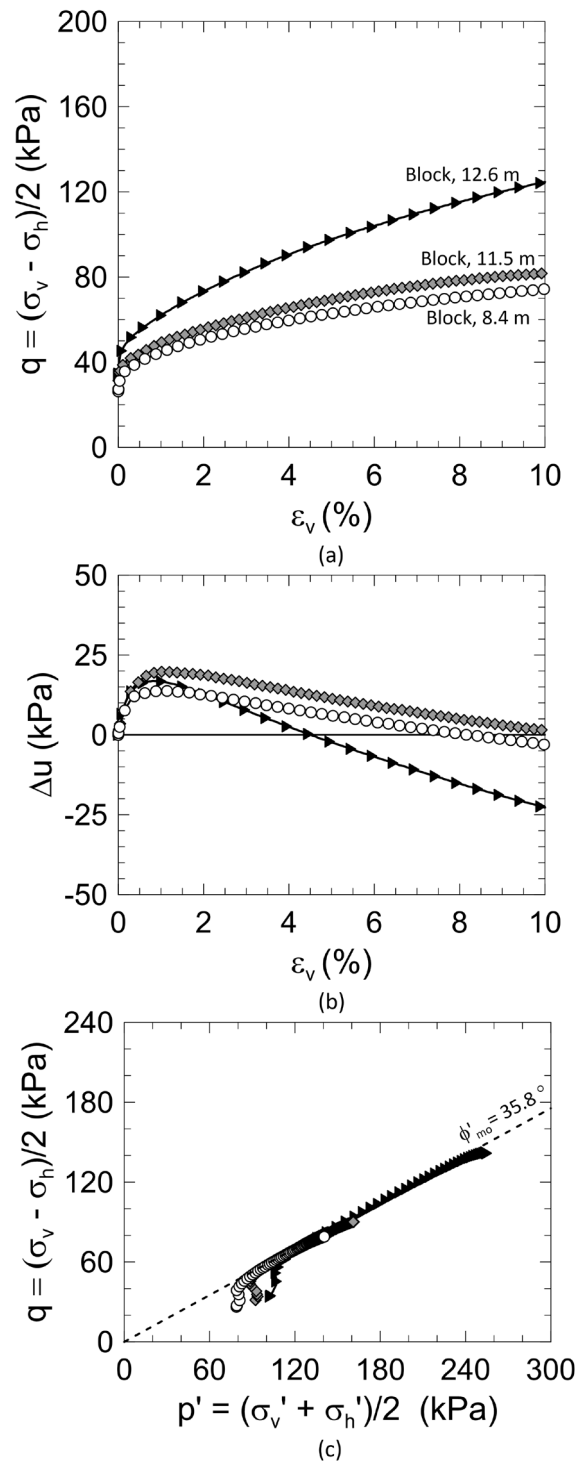


Figure 25. Typical CAUC test results from Halden block samples (HALB04) by means of (a) shear stress versus vertical strain, (b) shear-induced pore pressure versus vertical strain, and (c) stress-path plots. A strong tendency for dilative behavior develops negative shear induced pore pressure in the specimens and results in strain hardening upon shearing. As observed in other silts and intermediate soils no unique (peak) undrained shear strength is identified.

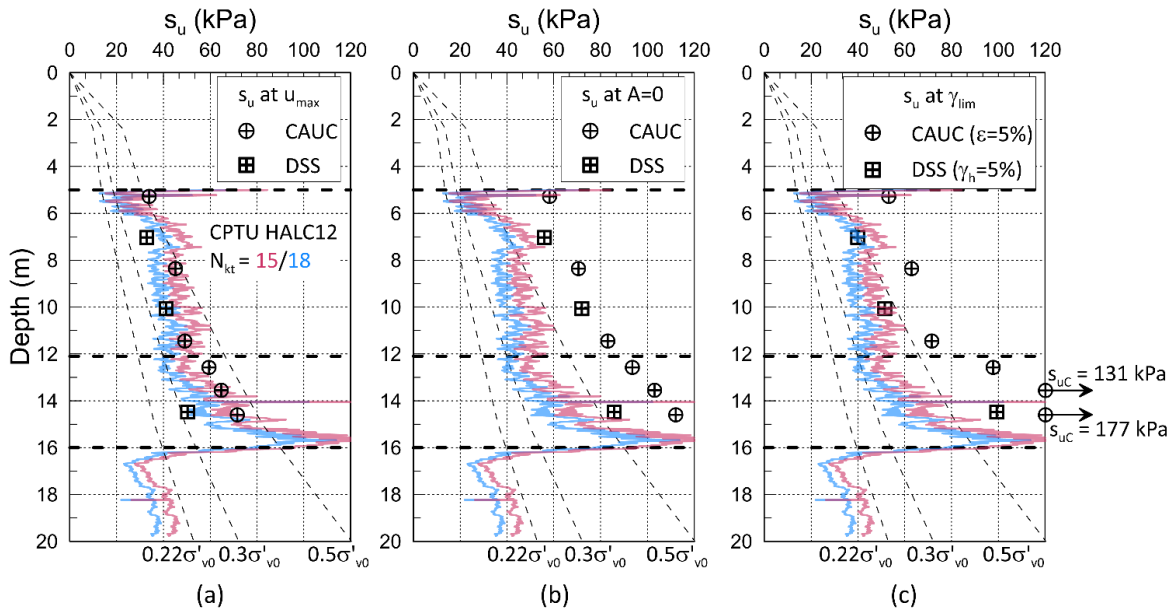


Figure 26. Results of CAUC and constant volume DSS tests on block samples of Halden silt. Undrained shear strength is interpreted as the shear stress at (a) maximum pore pressure, u_{max} , (b) $A=0$, and (c) a limiting shear strain of 5% in DSS and 5% axial strain in CAUC.

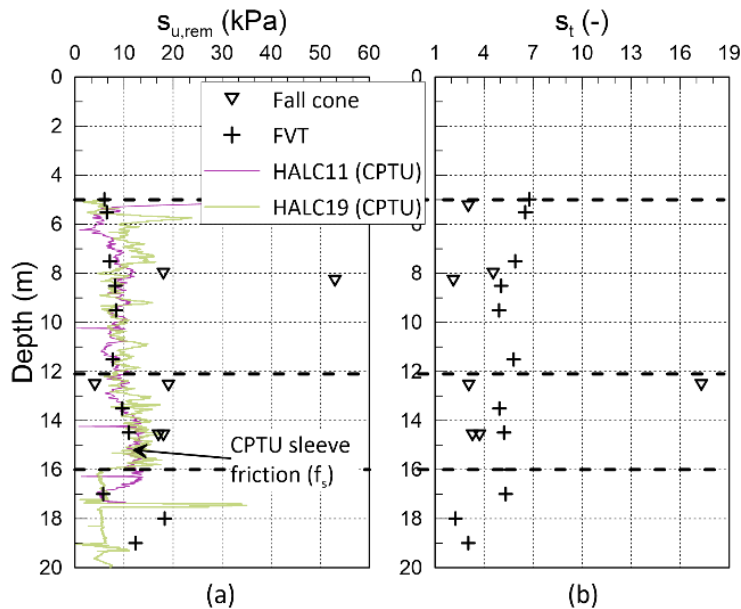


Figure 27. Results of (a) remolded undrained shear strength, and (b) sensitivity from fall cone and field vane tests.

6.14 Effective stress strength parameters

All soils are characterized by an effective stress friction envelope. This envelope is fundamental and referred to as the effective stress friction angle (ϕ' , ϕ'_{mo}), ideally obtained from drained triaxial tests in compression (CADC), but may also be assessed from undrained tests. The effective cohesion intercept (c') is not fundamental, but depends upon the yield surface, stress conditions, strain rate etc. Effective stress strength parameters are required for long term stability analyses. Figure 25c demonstrates that Halden silt has a consistent effective stress friction angle, ϕ'_{mo} , at maximum obliquity of about 36° in CAUC tests on block sample specimens with $c' = 0$. This friction angle is similar to results from drained tests. Friction angle values may also be assessed from CPTU data using e.g.:

- (i) The relationship between normalized cone resistance, Q_t and friction angle for uncemented, unaged, moderately compressible, predominately quartz sands [93]. The database was later corrected for calibration chamber boundary effects [94], and an alternative relationship presented as:

$$\phi' = 17.7^\circ + 11.0^\circ \times \log \left[\left(\frac{q_t / \sigma_{atm}}{\sigma'_{v0} / \sigma_{atm}} \right)^{0.5} \right] \quad (2)$$

- (ii) The NTH (now NTNU – Norwegian University of Science and Technology) limit plasticity approach [95,96], providing a relationship between normalized cone resistance number, N_m , the pore pressure ratio, B_q , and effective stress friction angle. For the simplified case, where the angle of plastification, β , and c' is taken as zero, an approximate expression for $B_q > 0.1$ becomes [68]:

$$\phi' = 29.5^\circ \times B_q^{0.121} \times (0.256 + 0.336 \cdot B_q + \log Q_t) \quad (3)$$

The two CPTU approaches are plotted with the laboratory data and DMT results in Figure 28. The DMT and CPTU correlations provide values that are significantly lower than the undrained triaxial test results. The DMT correlation of horizontal stress index, K_D to a friction angle, $\phi'_{safe,DMT}$ provides a lower bound estimate according to Marchetti [62]; in this case the value is typically in the range of 22° and 25° . The CPTU and DMT interpretations seem inappropriate, and the laboratory data is considered more reliable as they are broadly consistent with data reported by other researchers. $\phi' = 37^\circ$ – 40° are reported for Swedish silts [97,98], 32° – 35° for Norwegian silts [79,84], 28° – 39° for the American Mississippi Valley silt [92], and $\phi' = 40^\circ$ and greater for Irish silts [76,78].

6.15 Sample quality

An evaluation of sample quality should always be made while interpreting data from advanced geotechnical laboratory tests. Poor quality testing and sampling can adversely affect the interpreted engineering soil parameters, leading to poor geotechnical project performance and over or unsafe design. Methods developed to assess the quality of clay samples have existed for more than two decades, but there is still no established framework to quantify the degree of sampling disturbance in silts. The two conventional sample quality assessment frameworks using volumetric strain, ε_{vol} [99] and the normalized change in void ratio, $\Delta e/e_0$ [100] (where Δe is the change in void ratio upon reloading back to the in situ vertical effective stress, and e_0 is the initial void ratio.), with both evaluated during laboratory recompression to the estimated in situ effective stresses, must be treated with caution in silts for two reasons:

- (i) they were developed for clays, and in particular, the $\Delta e/e_0$ method for normally consolidated to medium overconsolidated marine clays. These frameworks may therefore not be valid for silts. In particular the $\Delta e/e_0$ criteria were developed based on results from laboratory tests performed on marine clays collected from depths below the seafloor of 0 m to 25 m and range in properties of 6% to 43% for plasticity index, 20% to 67% for water content, and 1 to 4 for OCR [100].
- (ii) loose silts may, if sheared drained or partially drained during tube sampling, densify and exhibit an artificially low change in void ratio upon recompression to in situ stresses, e.g. [76,84,101]. As such, certain samples may appear of high quality when they have in fact been significantly altered.

$\Delta e/e_0$ values for the CRS/IL oedometer, DSS and CAUC triaxial test on specimens from block samples collected at the Halden are presented in Figure 29a to Figure 29c. Essentially all values fall within the "very good to excellent" (1), or "good to fair" (2) categories. As described in Table 1 soil sampling using several other techniques (Geonor 54 mm fixed piston composite sampler, 72 mm fixed piston sampler and Gel-Push sampler) have been conducted at the site and interpretation of the results from these are in progress and will be reported in a subsequent paper.

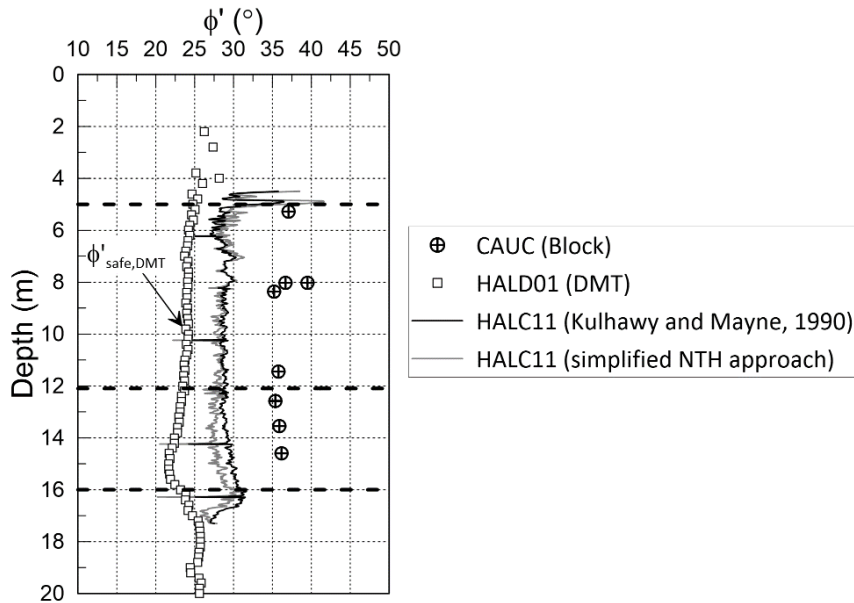


Figure 28. Interpretation of effective stress friction angle from DMT, CPTU, and laboratory CAUC tests on block samples.

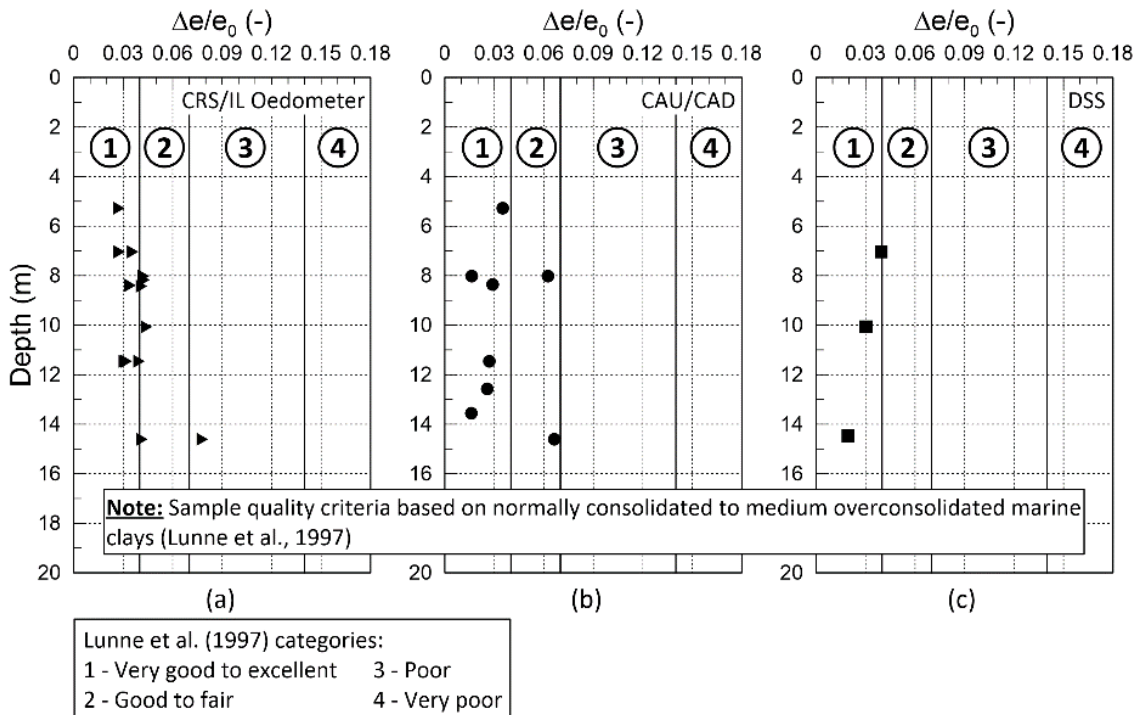


Figure 29. Evaluation of $\Delta e/e_0$ from (a) oedometer, (b) triaxial and (c) DSS testing on silt specimens from block samples.

7 Engineering problems

A discrepancy between in situ and laboratory results, and the lack of established correlations to important engineering parameters, are a few examples of the challenges faced during investigations of silts. While silts and other intermediate soils can complicate the design and construction phases of infrastructure projects both onshore and offshore, like in the North Sea e.g. [91,102], they lead to severe building damage during the 1999 Kocaeli earthquake [103] in Turkey. Knowledge of soil behavior and engineering properties in these materials is paramount, and research sites like Halden will assist the geotechnical profession to advance the state of the art. Some practical engineering problems related to soil sampling, in situ and laboratory testing at the Halden silt site are discussed below, including a slope failure case history from the neighboring wastewater treatment facility.

7.1 Soil sampling

Six sampling boreholes were drilled at the Halden site and sixty five samples collected. While the two Geonor fixed piston samplers collected 54 mm and 72 mm samples down to 16.5 m depth without any reported issues, the gel-push sampler equipment needed certain modifications to ensure compatibility with the NGI drill rig. When the appropriate modifications were made gel-push samples were successfully collected down to 13.4 m depth. After sampling the tube was left in the ground for several minutes to improve equalization of pore water pressure and reduce possible effects such as loss of part of the sample on retrieval from the base of the borehole. Full recovery was achieved in most cases during tube sampling. Some authors [78,79,84,101] report that conventional tube sampling in intermediate silty soils tend to compress or dilate the soil depending on the initial void ratio and prevailing drainage conditions upon shear. Dense silts may dilate upon tube sampling with a resulting increase in void ratio while looser silts may compress during sampling (decrease in the sample void ratio). At Halden, a study of the effects of sampler type on engineering parameters and laboratory behavior of silt is ongoing, but visual inspection of a number of samples revealed no obvious bending of soil strata or laminations in the peripheral zone near the tube sampler wall. This may also be due to the fact that the Halden silt shows little to no primary bedding and laminations due to bioturbation. Although limited research has been published on experience with block samples of silt some studies report hand carved blocks [76,104–106]. Sherbrooke block sampling has been conducted at Refneveien in Halden earlier [76], this site is approximately 500 m distance and 15 m lower in elevation from the Halden research site at Rødsparken described in this paper. Block sampling was successfully conducted at the Halden research site down to 15.2 m depth (see Figure 30a). On occasion, however, one or more of the spring-mounted blades were prevented from releasing by silt particles jamming the knives. As a result, the base of the block could not be properly separated from the bottom of the borehole and multiple attempts lead to disturbance of a few of the blocks. A second issue occurred as the blades retracted; in a few cases the friction between the knives and the silt at the base of the block would cause a wedge of soil to detach from the sample (Figure 30b). Similar issues

were encountered at Skibbereen in Ireland during tube sampling as a result of fines collection behind the piston head during sampling [76].

The lack of a reliable sample quality assessment framework for silts hinders determining which sampler could consistently provide a superior quality sample and hence better quality advanced laboratory test specimens. In the last few decades large diameter samples, e.g. Sherbrooke blocks [23] and Laval samples [107], have generally been considered superior to tube samples in clay. For silts further research on the efficacy of sampler type and sample sizes is needed.

7.2 Stress history

As demonstrated by the data presented herein, conducting oedometer tests on Halden silt specimens to assess stress history (σ'_p and OCR) serve limited purpose as the soil in this study was strain hardening immediately upon 1D loading in the CRS or IL cell. Thus determining if any preloading event occurred at the site was solely based on the geological background of the site, which in this case is well understood and documented. While, a classical Casagrande interpretation of yield stress from Halden oedometer test specimens results in an apparent overconsolidation ratio in the range of 2 to 5, it has been concluded herein that the true OCR is closer to 1, and except for some potential desiccation in the uppermost part of the soil profile, only aging and fluctuating ground water levels will have caused a yield stress slightly higher than the in situ vertical effective stress. Furthermore, classical CPTU correlations using factors established and validated for clays are inappropriate, misleading and in conflict with the depositional history of the site. For other silt sites, with limited knowledge of the geological background and no clay layers to assess, normally consolidated silts could be misinterpreted as overconsolidated if clay-based interpretation strategies are applied. Until more data on other silts worldwide are published, experiences from test sites such as Halden or Malamocco [7] may provide valuable information.

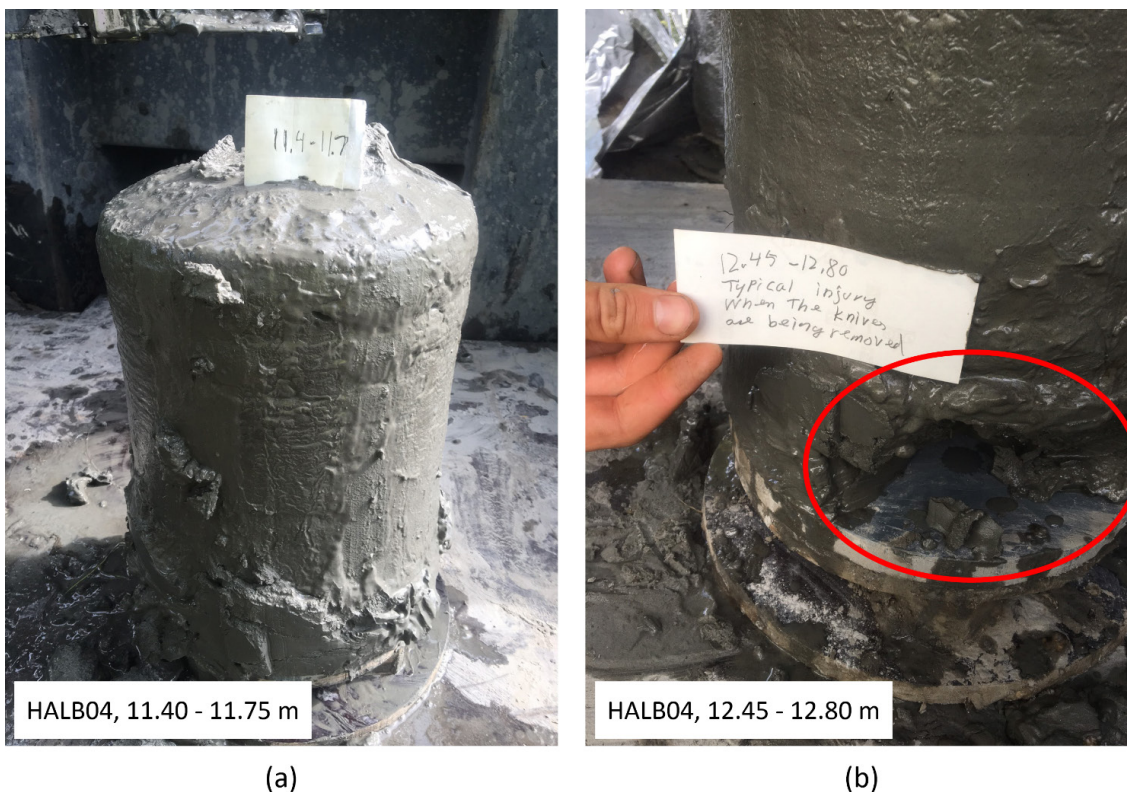


Figure 30. Sherbrooke block sampling of Halden silt (borehole HALB04); (a) Apparently good quality block from 11.5 m depth, (b) Damaged lower part of block from 12.4 m depth. Damage was caused by the retracting knives at the base of the block.

7.3 Partial drainage

Assessment of the prevailing drainage conditions in silts and other intermediate soils are particularly challenging. While for a certain foundation geometry and loading regime the soil response may be undrained, other combinations may act under partially-drained or fully drained conditions. This is also the case for in situ tests; depending on the rate of penetration, pore pressure dissipation may occur during testing. The influence of penetration rate and soil drainage properties (specifically the coefficient of consolidation) on the consolidation conditions in these soils are typically of great importance in design and can be captured by the normalized penetration velocity, $V = v \times d/c_h$, where v is the cone penetration rate, d is the penetrometer diameter and c_h is the horizontal coefficient of consolidation. Fully undrained penetration typically occurs when V is larger than about 30 to 100 and if less is typically associated with partially drained penetration. Fully drained penetration occurs when V is less than about 0.03 [108]. A CPTU penetration rate study conducted at Halden [85] demonstrated a clear increase in V with increased penetration rate as expected. While a reduced CPTU penetration rate (2 mm/s) resulted in V values in the region of 14–27, the conventional penetration rate of 20 mm/s yielded V values typically in the range of 95–273 in silt

Units II and III. This implies that undrained conditions are likely to prevail during standard cone penetration rate. It should be noted, however, that the suggested transition from undrained to partially drained conditions based on V or B_q at Halden are not in agreement. Excess pore pressures generated behind the cones in Halden are low ($B_q = 0.1\text{--}0.24$; Figure 14) and other researchers [96] have suggested that partially drained conditions prevail when $B_q < 0.4$. Further investigation of this topic is required for validation. As noted in Sections 6.3 and 6.9 the self-boring pressuremeter test, but also the dilatometer test, are rather slow in situ techniques compared to the CPTU. Thus, drainage or partial drainage could become a major factor and introduces uncertainty in the engineering parameters (e.g. K_0 and s_u) interpreted from these tests.

7.4 Case history: Remmen wastewater treatment facility

Slopes on silts are typically susceptible to landslides and local liquefaction under certain unfavorable conditions. Saturation may be high even above the free ground water table and the soils are quickly fully saturated if the water table increases [84]. This typically occurs during or after periods with significant rainfall or during spring when snow is melting. The ground water table rises and quickly saturates the overlying soils and breaks the matrix suction. This consequently reduces the effective stresses and strength of the soils. However, on slopes where negative pore pressures (suction) dominate, failures may not necessarily occur very often. Evaluations of the stability of these slopes, typically using overly conservative values of soil strength and in situ pore pressure, may underestimate the factor of safety against failure. Between 2009 and 2012 the Swedish Geotechnical Institute, SGI, performed monitoring of negative pore pressures on two silt slopes in Sweden [109,110]. The stability analyses of one of these slopes showed that by including suction in the calculations, the factor of safety increased by 5%–13%.

In the evening December 14th 2011 a local landslide was triggered up-slope from the Remmen wastewater treatment facility (RWTF), immediately west of the Halden research site (see Figure 31). For safety of the neighboring residents, the nearby properties (No. 8 and 10) were immediately evacuated. A broken water supply pipeline combined with a period of significant rainfall may have caused instabilities in the slope.

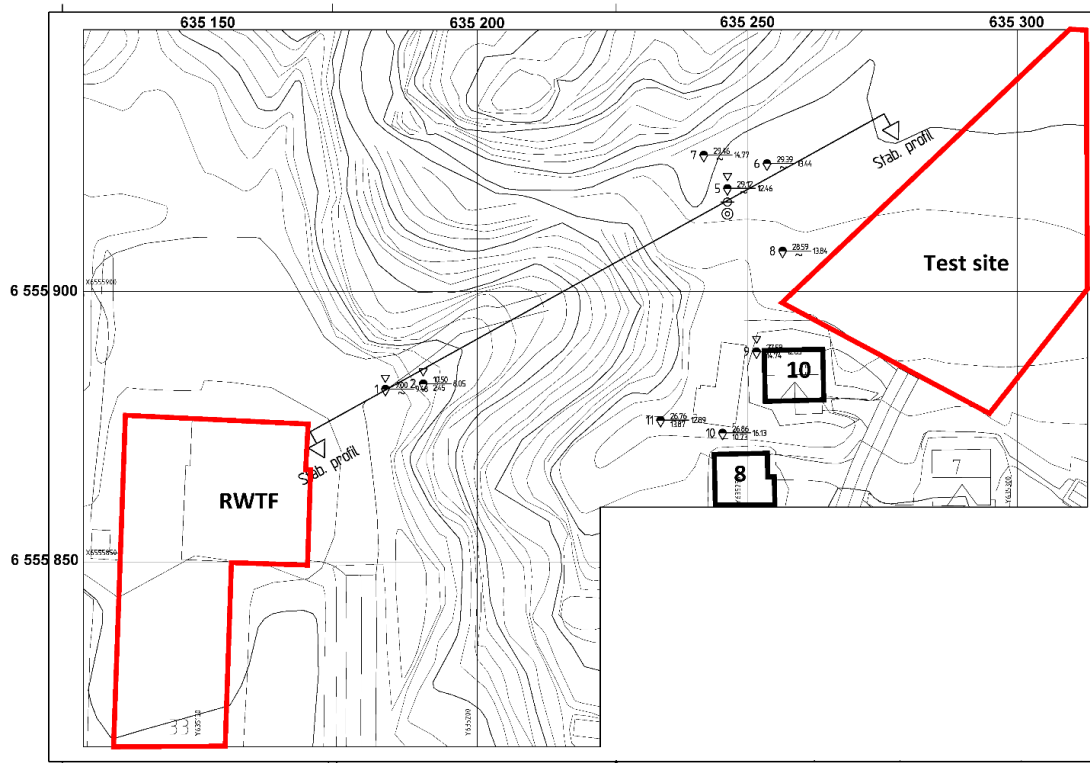


Figure 31. Location plan showing the Remmen wastewater treatment facility (RWTF) relative to the Halden research site, the slope in question and the neighboring houses (No. 8 and 10). Borehole locations 1, 2, 4 and 5 include cone penetration tests. 54 mm Geonor fixed piston sampling was conducted at location 5.

The topography slopes from an elevation of about 28 m above sea level at the crown of the slope to about 6 m at the toe (Figure 32). The width and depth of the slide was about 30 m and 3–4 m, respectively. The debris, estimated to a volume somewhere in the range of 1,000–2,000 m³ stopped just short of the treatment facility, about 80 m from the main scarp. NGI subsequently carried out the following soil investigation; 8 Norwegian total soundings, 3 CPTUs, installation of two piezometers and one sampling borehole on the slide crown using the Geonor 54 mm piston sampler. The field and laboratory testing revealed a clayey silt down to about 8 m depth, and 2 meters of silty clay over bedrock. Light detection and ranging (LiDAR) data from the site is also available from both pre- and post-failure. The elevation contours in Figure 33 shows that the debris have reached the access road and if only marginally greater, the landslide might have hit the exterior of the wastewater treatment facility and caused harm to infrastructure and people.

Effective stress slope stability calculations to assess the site conditions prior to failure were performed using the computer program BEAST [111] with 30 slices. In these analyses the silt was considered a granular material using an effective stress friction

angle. For a circular failure surface similar to the one observed in the field, and by applying $\phi' = 34^\circ$ ($c' = 0$ kPa) and $\phi' = 26^\circ$ ($c' = 5$ kPa) in the top sand and underlying silt, respectively, a factor of safety (FS) equal to 1.0 was obtained. At failure (FS = 1.0) the shear stresses (τ_{ff}) along the slip surface were generally in the range of 20 to 25 kPa.

Post-failure slope stability was still considered unacceptable and the probability of new slides considered high. To mitigate the risk of future hazards a dense grid of individual soilcrete columns were installed by means of deep soil mixing in the lower section of the slope. Deep soil mixing improves the strength characteristics by mechanically mixing the soil with a cementitious binder slurry, and as such the ground improvement stabilized the slope. Further, the soilcrete columns provided a foundation for the 1,500–2,000 m³ rock backfill now supporting the main scarp. The backfill is resistant to erosion and acts as counterweight. The FS after these measures was calculated to about 2.0.

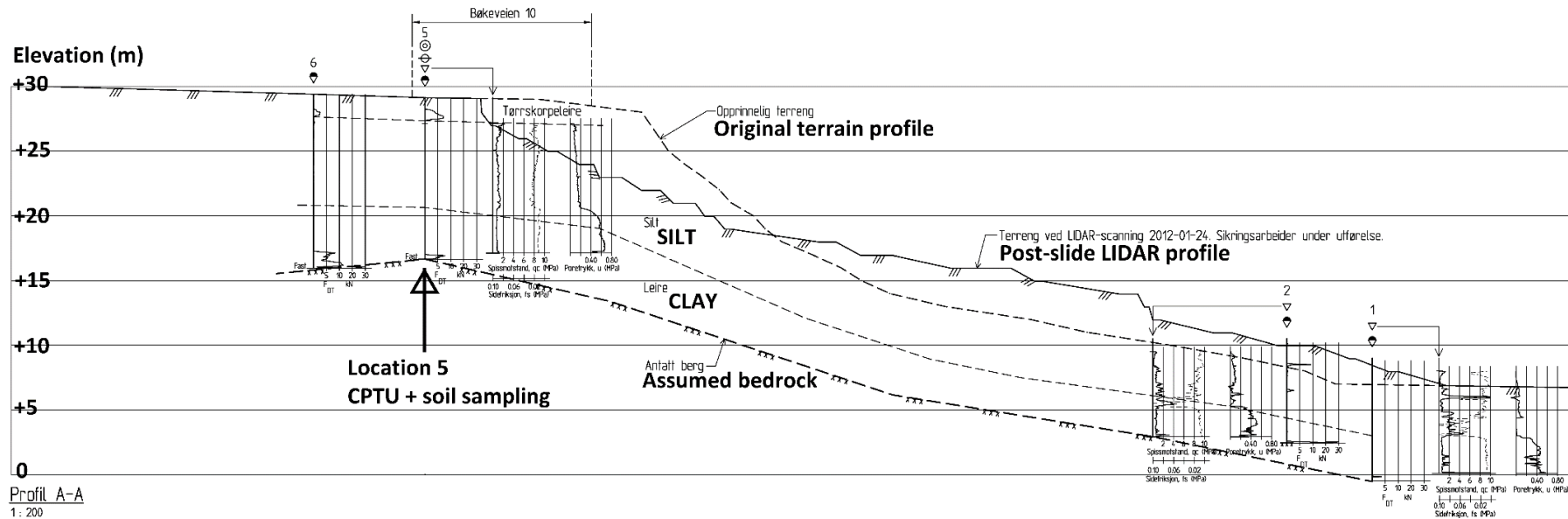


Figure 32. Cross-section showing original slope and post-failure slope profiles from North-West.

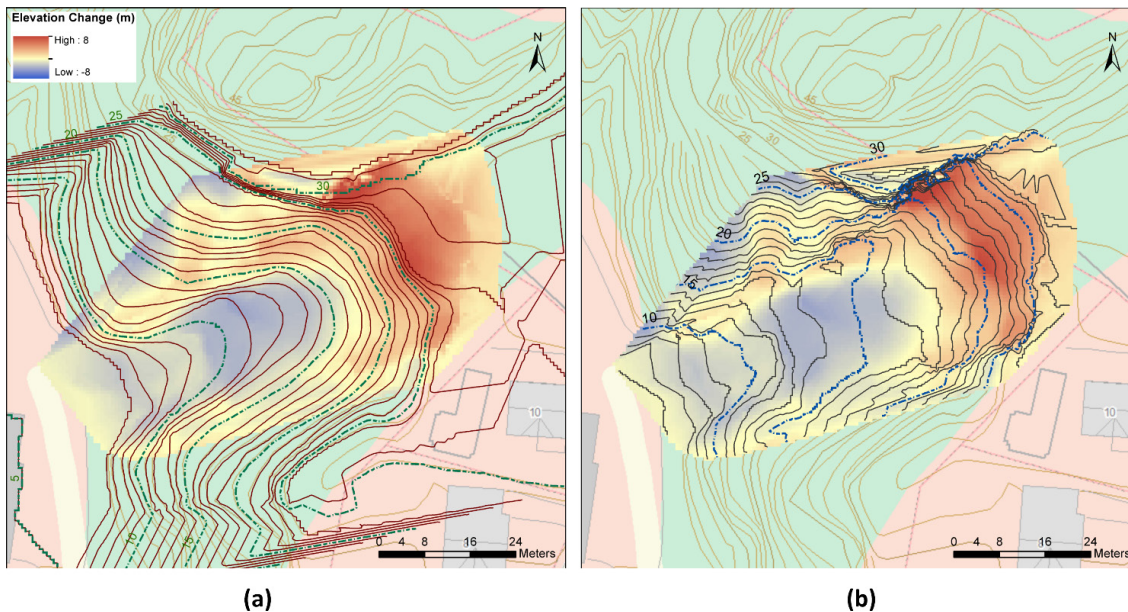


Figure 33. LiDAR results shows elevation contours of (a) Pre-failure conditions, and (b) post-failure conditions.

8 Summary and conclusions

Silts and similar intermediate soils represent a category of soils that are typically labelled challenging by geotechnical engineers. These soils can be difficult to sample, especially for very low plasticity to non-plastic silts, and there is no well-established framework to assess sample quality. Furthermore, little guidance is available on the selection of appropriate engineering properties for practical use. The Halden research site, located in Southeastern Norway, has been studied over a period of six years by combining the results of a number of geological, geophysical and geotechnical site investigation tools. The site emerged from the marine environment c. 5,000 years ago as a result of intense isostatic uplift and relative fall of sea-level. A silty, clayey sand constitutes the top soil and extends down to about 4.5 to 5 m depth. The clayey silt below is separated into two soil units based on the results of in situ and index tests, but is regarded as the same material with the same geologic origin and history. These extend down to about 15–16 m depth. Piezocone data reveals that the corrected cone resistance plots around 1 MPa, similar to that of the clay unit below, and excess pore pressures are generated behind the cones in the silt units. The pore pressure ratio is generally low, ranging between 0.1–0.3, and the soil behavior type index typically ranges between 2.6 and 2.95. The seismic cone results indicate a clear trend of increasing shear wave velocity with depth ranging from about 110 m/s at 2 m depth to 200 m/s at 16 m. Advanced CRS, CAUC and DSS laboratory testing revealed a number of challenges and limitations; (i) Methods developed to assess the quality of clay samples may not necessarily apply to these soils and there is no established framework to quantify the degree of sample disturbance in silts. (ii) Interpretation of the stress history based on both oedometer test results and

clay-based correlations to CPTU cone resistance are problematic and unreliable as they are in conflict the geological history in the area. Geology, and evidence of a normally consolidated stress state of the lower clay, suggests that also the silt is near normally consolidated. (iii) Undrained shear strengths, as interpreted from e.g. field vane tests, are consistent with the CPTU interpretations using $N_{kt} = 18$, but plot significantly lower than the results from undrained triaxial tests on block samples interpreted at large strain. The undrained triaxial tests exhibit a strong tendency for dilative behavior and provide no unique (peak) undrained shear strength. As a result, different strength criteria provide different results. Despite certain interpretation challenges the paper presents important reference data to assist in the interpretation and assessment of similar silts, and provide some guidance on important geotechnical properties for projects where limited design parameters are available.

References

1. Lacasse S, Berre T, Lefebvre G (1985) Block sampling of sensitive clay. In: Publications Committee of XI ICSMFE, editor. *Proceedings of the Eleventh International Conference on Soil Mechanics and Foundation Engineering, San Francisco, 12-16 August 1985*. Rotterdam: A.A. Balkema. pp. 887–892.
2. Lunne T, Long M, Forsberg CF (2003) Characterization and engineering properties of Onsøy clay. In: Tan TS, Phoon KK, Hight DW et al., editors. *Characterisation and Engineering Properties of Natural Soils*. Lisse: A.A. Balkema, 395–427.
3. Berre T, Lunne T, Andersen KH, et al. (2007) Potential improvements of design parameters by taking block samples of soft marine Norwegian clays. *Canadian Geotechnical Journal* 44: 698–716.
4. Berre T (2013) Test fill on soft plastic marine clay at Onsøy, Norway. *Canadian Geotechnical Journal* 51: 30–50.
5. Hight DW, Bond AJ, Legge JD (1992) Characterization of the Bothkennaar clay: an overview. *Géotechnique* 42: 303–347.
6. Ricceri G, Butterfield R (1974) An analysis of compressibility data from a deep borehole in Venice. *Géotechnique* 24: 175–192.
7. Cola S, Simonini P (2002) Mechanical behavior of silty soils of the Venice lagoon as a function of their grading characteristics. *Canadian Geotechnical Journal* 39: 879–893.
8. Low HE, Maynard ML, Randolph MF, et al. (2011) Geotechnical characterisation and engineering properties of Burswood clay. *Géotechnique* 61: 575–591.
9. Pineda JA, Suwal LP, Kelly RB, et al. (2016) Characterisation of Ballina clay. *Géotechnique* 66: 556-577.
10. Kelly RB, Pineda JA, Bates L, et al. (2017) Site characterisation for the Ballina field testing facility. *Géotechnique* 67: 279-300.
11. DeGroot DJ, Lutenege AJ (2003) Geology and engineering properties of Connecticut Valley Varved Clay. In: Tan TS, Phoon KK, Hight DW et al., editors. *Characterisation and Engineering Properties of Natural Soils*. Lisse: A.A. Balkema. pp. 695-724.
12. Lutenege AJ, Miller GA (1994) Uplift Capacity of Small-Diameter Drilled Shafts from In Situ Tests. *Journal of Geotechnical Engineering* 120: 1362-1380.
13. Briaud J-L, Gibbens R (1999) Behavior of Five Large Spread Footings in Sand. *Journal of Geotechnical and Geoenvironmental Engineering* 125: 787-796.

14. ISO (2002) Geotechnical investigation and testing - Identification and classification of soil. Part 1: Identification and description (ISO 14688-1). Geneva, Switzerland: International Organization for Standardization.
15. Norwegian Geotechnical Society (1989) Melding 7: Veiledning for utførelse av dreietrykksondering. Rev.1 [in Norwegian]. Oslo, Norway: Norwegian Geotechnical Society (NGF).
16. ISO (2012) Geotechnical investigation and testing - Field testing. Part 1: Electrical cone and piezocone penetration test (ISO 22476-1:2012). Geneva, Switzerland: International Organization for Standardization.
17. ISO (2017) Geotechnical investigation and testing - Field testing - Part 11: Flat dilatometer test (ISO 22476-11:2017). Geneva, Switzerland: International Organization for Standardization.
18. ISO (2012) Geotechnical investigation and testing - Field testing. Part 5: Flexible dilatometer test (ISO 22476-5:2012). Geneva, Switzerland: International Organization for Standardization.
19. Norwegian Geotechnical Society (2017) Melding 6: Veiledning for måling av grunnvannsstand og poretrykk. Rev. 2 [In Norwegian] Oslo, Norway: Norwegian Geotechnical Society (NGF).
20. Norwegian Geotechnical Society (1989) Melding 4: Veiledning for utførelse av vingeboring. Rev. 1 [in Norwegian]. Oslo, Norway: Norwegian Geotechnical Society (NGF).
21. Bjerrum L, Andersen KH (1972) In-situ measurements of lateral pressures in clay. *European Conference on Soil Mechanics and Foundation Engineering, 5 Madrid 1972 Proceedings*. Madrid: Sociedad Española de Mecánica del Suelo y Cimentaciones.
22. Norwegian Geotechnical Society (2013) Melding 11: Veiledning for prøvetaking [In Norwegian]. Oslo, Norway: Norwegian Geotechnical Society (NGF).
23. Lefebvre G, Poulin C (1979) A new method of sampling in sensitive clay. *Canadian Geotechnical Journal* 16: 226-233.
24. Emdal A, Gylland A, Amundsen HA, et al. (2016) Mini-block sampler. *Canadian Geotechnical Journal* 53: 1235-1245.
25. Huang AB, Tai YY, Lee WF, et al. (2008) Sampling and field characterization of the silty sand in Central and Southern Taiwan. In: Huang AB, Mayne PW, editors. *Geotechnical and Geophysical Site Characterization*. Leiden: Taylor & Francis. pp. 1457-1463.

26. Kazuo T, Kaneko S (2006) Undisturbed sampling method using thick water-soluble polymer solution Tsuchi-to-Kiso. *Journal of the Japanese Geotechnical Society [In Japanese]* 54: 145-148.
27. ISO (2014) Geotechnical investigation and testing - Laboratory testing of soil. Part 1: Determination of water content (ISO 17892-1). Geneva, Switzerland: International Organization for Standardization.
28. ISO (2014) Geotechnical investigation and testing - Laboratory testing of soil. Part 2: Determination of bulk density (ISO 17892-2). Geneva, Switzerland: International Organization for Standardization.
29. ISO (2015) Geotechnical investigation and testing - Laboratory testing of soil. Part 3: Determination of particle density (ISO 17892-3). Geneva, Switzerland: International Organization for Standardization.
30. ISO (2018) Geotechnical investigation and testing - Laboratory testing of soil. Part 12: Determination of liquid and plastic limits (ISO 17892-12). Geneva, Switzerland: International Organization for Standardization.
31. Mow J (1965) Falling drop used for grain-size analysis of fine-grained materials. *Sedimentology* 5: 343-347.
32. ISO (2016) ISO (2015) Geotechnical investigation and testing - Laboratory testing of soil. Part 4: Determination of particle size distribution (ISO 17892-4). Geneva, Switzerland: International Organization for Standardization.
33. NS (1988) Geotechnical testing - Laboratory methods. Determination of undrained shear strength by fall-cone testing (NS 8015). Oslo, Norway: Standards Norway.
34. ISO (1994) Soil quality. Determination of the specific electrical conductivity (ISO 11265). Geneva, Switzerland: International Organization for Standardization.
35. ISO (2017) Geotechnical investigation and testing - Laboratory testing of soil. Part 5: Incremental loading oedometer test (ISO 17892-5) Geneva, Switzerland: International Organization for Standardization.
36. Sandbækken G, Berre T, Lacasse S (1986) Oedometer Testing at The Norwegian Geotechnical Institute. In: Yong RN, Townsend FC, editors. *Consolidation of soils: testing and evaluation, STP 892*: American Society for Testing and Materials. pp. 329-353.
37. NS (1993) Geotechnical testing - Laboratory methods. Determination of one-dimensional consolidation properties by oedometer testing - Method using continuous loading (NS 8018). Oslo, Norway: Standards Norway.

38. ISO (2004) Geotechnical investigation and testing - Laboratory testing of soil. Part 11: Determination of permeability by constant and falling head (ISO/TS 17892-11). Geneva, Switzerland: International Organization for Standardization.
39. Wang Z, Gelius L-J, Kong F-N (2009) Simultaneous core sample measurements of elastic properties and resistivity at reservoir conditions employing a modified triaxial cell – a feasibility study. *Geophysical Prospecting* 57: 1009-1026.
40. Berre T (1982) Triaxial Testing at the Norwegian Geotechnical Institute. *Geotechnical Testing Journal* 5: 3-17.
41. ISO (2018) Geotechnical investigation and testing - Laboratory testing of soil. Part 9: Consolidated triaxial compression tests on water saturated soils (ISO 17892-9). Geneva, Switzerland: International Organization for Standardization.
42. Bjerrum L, Landva A (1966) Direct Simple-Shear Tests on a Norwegian Quick Clay. *Géotechnique* 16: 1-20.
43. ASTM (2015) Standard Test Method for Consolidated Undrained Direct Simple Shear Testing of Fine Grain Soils (ASTM D6528-17). West Conshohocken, PA: ASTM International.
44. Dyvik R, Madshus C (1985) Lab measurements of Gmax using bender elements. In: Khosla V, editor. *Advances in the Art of Testing Soils under Cyclic Conditions: Proceedings of a Session in Conjunction with the ASCE Convention in Detroit, Michigan 1985*. New York: American Society of Civil Engineers. pp. 186-196.
45. Sørensen R (1999) En 14C datert og dendrokronologisk kalibrert strandforskyvningskurve for søndre Østfold, Sørøst-Norge [In Norwegian]. In: Selsing L, Lillehammer G, editors. *Museumslandskap: artikkelsamling til Kerstin Griffin på 60-årsdagen*. Stavanger: Arkeologisk museum i Stavanger. pp. 59-70.
46. Klemsdal T (2002) Landformene i Østfold [In Norwegian]. *Natur i Østfold* 21: 7-31.
47. Olsen L, Sørensen E (1993) Halden 1913 II, Quaternary map, 1:50.000, with descriptions (in Norwegian). Trondheim: Geological Survey of Norway.
48. Sørensen R (1979) Late Weichselian deglaciation in the Oslofjord area, south Norway. *Boreas* 8: 241-246.
49. Kenney TC (1964) Sea-Level Movements and the Geologic Histories of the Post-Glacial Marine Soils at Boston, Nicolet, Ottawa and Oslo. *Géotechnique* 14: 203-230.
50. Ostendorf DW, DeGroot DJ, Shelburne WM, et al. (2004) Hydraulic head in a clayey sand till over multiple timescales. *Canadian Geotechnical Journal* 41: 89-105.

51. Norwegian Geotechnical Society (2011) Melding 2: Veiledning for symboler og definisjoner i geoteknikk - Identifisering og klassifisering av jord. Rev. 2 [In Norwegian]. Oslo, Norway: Norwegian Geotechnical Society (NGF).
52. Pettijohn FJ (1949) *Sedimentary Rocks*. New York: Harper and Row.
53. Rosenqvist IT (1975) Origin and Mineralogy Glacial and Interglacial Clays of Southern Norway. *Clays and Clay Minerals* 23: 153-159.
54. Solberg IL, Hansen L, Rønning JS, et al. (2012) Combined geophysical and geotechnical approach to ground investigations and hazard zonation of a quick clay area, mid Norway. *Bulletin of Engineering Geology and the Environment* 71: 119-133.
55. Solberg I-L, Rønning JS, Dalsegg E, et al. (2008) Resistivity measurements as a tool for outlining quick-clay extent and valley-fill stratigraphy: a feasibility study from Buvika, central Norway. *Canadian Geotechnical Journal* 45: 210-225.
56. Hansen L, L'heureux JS, Longva O (2011) Turbiditic, clay-rich event beds in fjord-marine deposits caused by landslides in emerging clay deposits – palaeoenvironmental interpretation and role for submarine mass-wasting. *Sedimentology* 58: 890-915.
57. Norwegian Geotechnical Institute (2002) Early Soil Investigations for Fast Track Projects: Assessment of Soil Design Parameters from Index Measurements in Clays. Summary Report/Manual 521553-3. Oslo: Norwegian Geotechnical Institute.
58. Norwegian Geotechnical Society (2010) Melding 5: Veiledning for utførelse av trykksondering. Rev. 3 [in Norwegian]. Oslo, Norway: Norwegian Geotechnical Society (NGF).
59. Lunne T, Strandvik SO, Kåsin K, et al. (2018) Effect of cone penetrometer type on CPTU results at a soft clay test site in Norway. In: Hicks MA, Pisanò F, Peuchen J, editors. *Cone Penetration Testing 2018*. Leiden: CRC Press. pp. 417-422.
60. Robertson PK (1990) Soil classification using the cone penetration test. *Canadian Geotechnical Journal* 27: 151-158.
61. Marchetti S (1980) In Situ Tests by Flat Dilatometer. *Journal of the Geotechnical Engineering Division, ASCE* 106: 299-321.
62. Marchetti S, Monaco P, Totani G, et al. (2006) The Flat Dilatometer Test (DMT) in soil investigations A Report by the ISSMGE Committee TC16. In: Failmezger RA, Anderson JB, editors. *Proceedings from the Second International Conference on the Flat Dilatometer, Washington, DC, April 2-5, 2006*. Lancaster, VA: In-Situ Soil Testing.
63. Marsland A, Randolph MF (1977) Comparisons of the results from pressuremeter tests and large in situ plate tests in London Clay. *Géotechnique* 27: 217-243.

64. Casagrande A (1936) The determination of the preconsolidation load and its practical significance. *Proceedings of the First International Conference on Soil Mechanics and Foundation Engineering: Cambridge, MA, 22-26 June 1936*. Cambridge: Graduate school of engineering, Harvard University. pp. 60-64.
65. Janbu N (1963) Soil compressibility as determined by oedometer and triaxial tests. *Problems of Settlements and Compressibility of Soils: Proceedings: European Conference of Soil Mechanics and Foundation Engineering, Wiesbaden, Germany*. pp. 19-25.
66. Pacheco Silva F (1970) A new graphical construction for determination of the pre-consolidation stress of a soil sample. *Proceedings of the 4th Brazilian Conference on Soil Mechanics and Foundation Engineering, Rio de Janeiro, Brazil*. pp. 225-232.
67. Lunne T, Robertson PK, Powell JJM (1997) Cone penetration testing in geotechnical practice. London: Blackie Academic & Professional.
68. Mayne PW (2007) Cone Penetration Testing: A Synthesis of Highway Practice. NCHRP Synthesis 368. Washington, D.C.: Transportation Research Board.
69. Chandler RJ (1988) The In-Situ Measurement of the Undrained Shear Strength of Clays Using the Field Vane. In: Richards AF, editor. *Vane Shear Strength Testing in Soils: Field and Laboratory Studies, STP 1014*. West Conshohocken, PA: ASTM International. pp. 13-32.
70. Mesri G, Hayat TM (1993) The coefficient of earth pressure at rest. *Canadian Geotechnical Journal* 30: 647-666.
71. Palmer AC (1972) Undrained plane-strain expansion of a cylindrical cavity in clay: a simple interpretation of the pressuremeter test. *Géotechnique* 22: 451-457.
72. Wroth CP (1984) The interpretation of in situ soil tests. *Géotechnique* 34: 449-489.
73. Rix GJ, Stoke KH (1991) Correlation of Initial Tangent Modulus and Cone Resistance. In: Huang AB, editor. *Calibration Chamber Testing: Proceedings of the First International Symposium (ISOCCTI), Potsdam, NY, USA, 28-29 June, 1991*: Elsevier. pp. 351-362.
74. Mayne PW, Rix GJ (1995) Correlations between shear wave velocity and cone tip resistance in natural clays. *Soils and Foundations* 35: 107-110.
75. Janbu N (1985) Soil models in offshore engineering. *Géotechnique* 35: 241-281.
76. Carroll R, Long M (2017) Sample Disturbance Effects in Silt. *Journal of Geotechnical and Geoenvironmental Engineering* 143: 04017061.
77. Martins FB, Bressani LA, Coop MR, et al. (2001) Some aspects of the compressibility behaviour of a clayey sand. *Canadian Geotechnical Journal* 38: 1177-1186.

78. Long M (2007) Engineering characterization of estuarine silts. *Quarterly Journal of Engineering Geology and Hydrogeology* 40: 147-161.
79. Long M, Gudjonsson G, Donohue S, et al. (2010) Engineering characterisation of Norwegian glaciomarine silt. *Engineering Geology* 110: 51-65.
80. Skúlasson J (1996) Settlement investigation on Icelandic silt. In: Erlingsson S, Sigursteinsson H, editors. *Interplay between geotechnics and environment : XII Nordic Geotechnical Conference, NGM-96, Reykjavik, 1996*. Reykjavik: Jarðtæknifélag Íslands. pp. 435–441.
81. DeJong JT, Jaeger RA, Boulanger RW, et al. (2013) Variable penetration rate cone testing for characterization of intermediate soils. In: Coutinho RQ, Mayne PW, editors. *Geotechnical and Geophysical Site Characterization 4*. Boca Raton, FL: Taylor & Francis. pp. 25-42.
82. Taylor DW (1948) *Fundamentals of soil mechanics*. New York: J. Wiley.
83. Ladd CC, Weaver JS, Germaine JT, et al. (1985) Strength-Deformation Properties of Arctic Silt. In: F. Lawrence Bennett, Jerry L. Machemehl, Thelen NDW, editors. *Civil Engineering in the Arctic Offshore: Conference Arctic '85, San Francisco, CA, March 25-27, 1985*. New York: American Society of Civil Engineers. pp. 820–829.
84. Sandven R (2003) Geotechnical properties of a natural silt deposit obtained from field and laboratory tests. In: Tan TS, Phoon KK, Hight DW et al., editors. *Characterisation and Engineering Properties of Natural Soils*. Lisse: A.A. Balkema. pp. 1121–1148.
85. Carroll R, Paniagua López AP (2018) Variable rate of penetration and dissipation test results in a natural silty soil. In: Hicks MA, Pisanò F, Peuchen J, editors. *Cone Penetration Testing 2018: Proceedings of the 4th International Symposium on Cone Penetration Testing (CPT'18), 21-22 June, 2018, Delft, The Netherlands*. London: CRC Press.
86. Sully JP, Robertson PK, Campanella RG, et al. (1999) An approach to evaluation of field CPTU dissipation data in overconsolidated fine-grained soils. *Canadian Geotechnical Journal* 36: 369-381.
87. Larsson R (1997) Investigations and load tests in silty soils. Results from a series of investigations in silty soils in Sweden. Report 54. Linköping: Swedish Geotechnical Institute, SGI. 257 p.
88. Blight GE (1968) A Note on Field Vane Testing of Silty Soils. *Canadian Geotechnical Journal* 5: 142-149.
89. Gibson RE, Anderson WF (1961) In situ measurement of soil properties with the pressuremeter *Civil Engineering and Public Works Review* 56: 615-618.

90. Aubeny CP, Whittle AJ, Ladd CC (2000) Effects of Disturbance on Undrained Strengths Interpreted from Pressuremeter Tests. *Journal of Geotechnical and Geoenvironmental Engineering* 126: 1133-1144.
91. Senneset K, Sandven R, Lunne T, et al. (1988) Piezocone tests in silty soils. In: de Ruiter J, editor. *Penetration testing, 1988: proceedings of the First International Symposium on Penetration Testing, ISOPT-1, Orlando, 20-24 March 1988*. Rotterdam, The Netherlands: A.A. Balkema. pp. 863-870.
92. Brandon TL, Rose AT, Duncan JM (2006) Drained and undrained strength interpretation for low-plasticity silts. *Journal of Geotechnical and Geoenvironmental Engineering* 132: 250-257.
93. Robertson PK, Campanella RG (1983) Interpretation of cone penetration tests. Part I: Sand. *Canadian Geotechnical Journal* 20: 734–745.
94. Kulhawy FH, Mayne PW (1990) Manual on Estimating Soil Properties for Foundation Design. Report EL-6800. Electric Power Research Institute. Palo Alto, CA.
95. Janbu N, Senneset K (1974) Effective stress interpretation of in-situ static penetration tests. *Proceedings of the European Symposium on Penetration Testing, ESOPT, Stockholm, June 5-7, 1974*. Stockholm: National Swedish Building Research. pp. 181–193.
96. Senneset K, Sandven R, Janbu N (1989) Evaluation of soil parameters from piezocone tests. *Transportation Research Record* 1235: 24–37.
97. Börgesson L (1981) Shear strength of inorganic silty soils. *Proceedings of the 10th International Conference on Soil Mechanics and Foundation Engineering: 15-19 June, Stockholm, 1981*. Rotterdam: A.A. Balkema. pp. 567–572.
98. Høeg K, Dyvik R, Sandbækken G (2000) Strength of undisturbed versus reconstituted silt and silty sand specimens. *Journal of Geotechnical and Geoenvironmental Engineering* 126: 606-617.
99. Terzaghi K, Peck RB, Mesri G (1996) Soil Mechanics in Engineering Practice: John Wiley and Sons.
100. Lunne T, Berre T, Strandvik S (1997) Sample disturbance effects in soft low plastic Norwegian clay. In: Almeida M, editor. *Recent Developments in Soil and Pavement Mechanics: Proceedings of the International Symposium, Rio de Janeiro, Brazil, 25-27 June 1997*. Rotterdam: A.A. Balkema. pp. 81–102.
101. Hight DW, Leroueil S (2003) Characterisation of soils for engineering purposes,. In: Tan TS, Phoon KK, Hight DW et al., editors. *Characterisation and Engineering Properties of Natural Soils*. Lisse: A.A. Balkema. pp. 255–360.

102. Solhjell E, Strandvik SO, Carroll R, et al. (2017) Johan Sverdrup–Assessment of soil material behaviour and strength properties for the shallow silt layer. *Offshore Site Investigation and Geotechnics, Smarter Solutions for Future Offshore Developments: Proceedings of the 8th International Conference 12-14 September 2017 Royal Geographical Society, London, UK*. London: Society for Underwater Technology. pp. 1275–1282.
103. Bray JD, Sancio RB, Durgunoglu T, et al. (2004) Subsurface Characterization at Ground Failure Sites in Adapazari, Turkey. *Journal of Geotechnical and Geoenvironmental Engineering* 130: 673–685.
104. Arroyo M, Pineda JA, Sau N, et al. (2015) Sample quality examination in silty soils. In: Winter MG, Smith DM, Eldred PJJ et al., editors. *Geotechnical engineering for infrastructure and development : proceedings of the XVI European Conference on Soil Mechanics and Geotechnical Engineering*. London: ICE Publishing. pp. 2873–2878.
105. Bradshaw AS, Baxter CDP (2007) Sample Preparation of Silts for Liquefaction Testing. *Geotechnical Testing Journal* 30: 324–332.
106. Sau N, Arroyo M, Pérez N, et al. (2014) Using CAT to obtain density maps in Sherbrooke specimens of silty soils. In: Soga K, Kumar K, Biscontin G et al., editors. *Geomechanics from micro to macro: proceedings of the TC105 ISSMGE International Symposium on Geomechanics from Micro to Macro, Cambridge, UK, 1-3 September 2014*. Leiden, Netherlands: CRC Press. pp. 1153–1158.
107. LaRochelle P, Sarrailh J, Tavenas F, et al. (1981) Causes of sampling disturbance and design of a new sampler for sensitive soils. *Canadian Geotechnical Journal* 18: 52-66.
108. DeJong JT, Randolph M (2012) Influence of Partial Consolidation during Cone Penetration on Estimated Soil Behavior Type and Pore Pressure Dissipation Measurements. *Journal of Geotechnical and Geoenvironmental Engineering* 138: 777–788.
109. Vesterberg B, Bertilsson R, Löfroth H (2017) Photographic feature: Monitoring of negative porewater pressure in silt slopes. *Quarterly Journal of Engineering Geology and Hydrogeology* 50: 245–248.
110. Westerberg B, Bertilsson R, Prästings A, et al. (2014) Publication 9: Negativa portryck och stabilitet i siltslänter. Linköping: Statens Geotekniska Institut, SGI [in Swedish, with summary in English].
111. Clausen CJF (2003) BEAST. A computer program for limit equilibrium analysis by method of slices. Report 8302-2. Rev. 4, 24 April.



Dokumentinformasjon/Document information		
Dokumenttittel/Document title Halden research site - Site characterisation and engineering properties of Halden silt		Dokumentnr./Document no. 20160154-05-R
Dokumenttype/Type of document Rapport / Report	Oppdragsgiver/Client Research Council of Norway (RCN)	Dato/Date 2019-10-02
Rettigheter til dokumentet iht kontrakt/ Proprietary rights to the document according to contract NGTS		Rev.nr.&dato/Rev.no.&date 0 /
Distribusjon/Distribution ÅPEN: Skal tilgjengeliggjøres i åpent arkiv (BRAGE) / OPEN: To be published in open archives (BRAGE)		
Emneord/Keywords Norwegian GeoTest Sites, Silt, Field, Lab		

Stedfesting/Geographical information	
Land, fylke/Country Norway, Østfold	Havområde/Offshore area -
Kommune/Municipality Halden	Felt navn/Field name -
Sted/Location Halden	Sted/Location -
Kartblad/Map	Felt, blokknr./Field, Block No. -
UTM-koordinater/UTM-coordinates Zone: East: North:	Koordinater/Coordinates Projection, datum: East: North:

Dokumentkontroll/Document control					
Kvalitetssikring i henhold til/Quality assurance according to NS-EN ISO9001					
Rev/Rev.	Revisjonsgrunnlag/Reason for revision	Egenkontroll av/ Self review by:	Sidemanns-kontroll av/ Colleague review by:	Uavhengig kontroll av/ Independent review by:	Tverrfaglig kontroll av/ Interdisciplinary review by:
0	Original document	2019-06-12 Øyvind Blaker	2019-10-02 Priscilla Paniagua		

Dokument godkjent for utsendelse/ Document approved for release	Dato/Date 2 October 2019	Prosjektleder/Project Manager Jean-Sebastien L'Heureux
--	------------------------------------	--

